Elevated gas flux and trace metal degassing from the 2014-2015 fissure eruption at the Bárðarbunga volcanic system, Iceland

Pierre-Jean Gauthier, Olgeir Sigmarsson, Mathieu Gouhier, Baptiste Haddadi, Séverine Moune

AGU PUBLICATIONS

JGR

Journal of Geophysical Research: Solid Earth

RESEARCH ARTICLE
10.1002/2015JB012111

Key Points:
- Satellite data and the petrologic method yield coherent SO_2 flux of ~1130 kg/s
- Trace element volatility is moderate as at other hot spot volcanoes
- Radioactive disequilibria suggest fast magma transfer to the eruption site

Supporting Information:
- Supporting Information S1
- Figure S1

Correspondence to:
P.-J. Gauthier,
P.J.Gauthier@opgc.fr

Citation:
Gauthier, P.-J., O. Sigmarsson, M. Gouhier, B. Haddadi, and S. Moune (2016), Elevated gas flux and trace metal degassing from the 2014–2015 fissure eruption at the Bárðarbunga volcanic system, Iceland, *J. Geophys. Res. Solid Earth*, *121*, 1610–1630, doi:10.1002/2015JB012111.

Received 20 APR 2015
Accepted 14 FEB 2016
Accepted article online 18 FEB 2016
Published online 23 MAR 2016

Elevated gas flux and trace metal degassing from the 2014–2015 fissure eruption at the Bárðarbunga volcanic system, Iceland

Pierre-Jean Gauthier[1], Olgeir Sigmarsson[1,2], Mathieu Gouhier[1], Baptiste Haddadi[1], and Séverine Moune[1]

[1]Laboratoire Magmas et Volcans, Université Blaise Pascal-CNRS-IRD, OPGC, Aubière, France, [2]Institute of Earth Sciences, University of Iceland, Reykjavik, Iceland

Abstract The 2014 Bárðarbunga rifting event in Iceland resulted in a 6-month long eruption at Holuhraun. This eruption was characterized by high lava discharge rate and significant gas emission. The SO_2 flux for the first 3 months was measured with satellite sensors and the petrologic method. High-resolution time series of the satellite data give 1200 kg/s that concurs with 1050 kg/s obtained from melt inclusion minus degassed lava sulfur contents scaled to the mass of magma produced. A high-purity gas sample, with elevated S/Cl due to limited chlorine degassing, reveals a similar degassing pattern of trace metals as observed at Kīlauea (Hawai'i) and Erta Ale (Ethiopia). This suggests a common degassing mechanism at mantle plume-related volcanoes. The trace metal fluxes, calculated from trace element to sulfur ratios in the gas sample and scaled to the sulfur dioxide flux, are 1–2 orders of magnitude stronger at Holuhraun than Kīlauea and Erta Ale. In contrast, volcanoes at convergent margins (Etna and Stromboli, Italy) have 1–2 orders of magnitude higher trace element fluxes, most likely caused by abundant chlorine degassing. This emphasizes the importance of metal degassing as chlorine species. Short-lived disequilibria between radon daughters, ^{210}Pb-^{210}Bi-^{210}Po measured in the gas, suggest degassing of a continuously replenished magma batch beneath the eruption site. Earlier and deep degassing phase of carbon dioxide and polonium is inferred from low ($^{210}Po/^{210}Pb$) in the gas, consistent with magma transfer rate of 0.75 m/s.

1. Introduction

Volcanic gases released during open vent passive degassing and sustained eruptions are a major source of volatile species directly injected into the atmosphere. Remote sensing measurement of sulfur dioxide (SO_2) fluxes is easier than that of the more abundant water vapor and carbon dioxide [*Pyle et al.*, 2013, and references therein]. While the global emission rate of SO_2 is reasonably well established, gas fluxes from volcanoes above mantle plumes are less well known than those at convergent margins. At Kīlauea volcano, Hawai'i, satellite measurements reveal a SO_2 flux of approximately 9–21 kt/d [*Beirle et al.*, 2014], which exceeds by a factor 2 to 5 values obtained from regular ground-based measurements [*Elias and Sutton*, 2012]. Ground-based measurements for persistent degassing activity at active lava lakes only yield 0.11 kt/d at Erta Ale, Ethiopia [*Oppenheimer et al.*, 2004] and less than 80 t/d at Mount Erebus, Antarctica [*Boichu et al.*, 2010]. In contrast, the sulfur release during discrete eruptive events may be significantly higher and reached, for instance, up to 100 kt/d during the 2007 eruption at Piton de la Fournaise, Reunion Island [*Gouhier and Coppola*, 2011] and approximately 200 kt/d at Sierra Negra, Galapagos, in 2005 [*Thomas et al.*, 2009]. Moreover, the 2010 Eyjafjallajökull (Iceland) eruption released up to 200 kt/d of SO_2 into the atmosphere, as determined with Infrared Atmospheric Sounding Interferometer (IASI) data [*Carboni et al.*, 2012]. On a different scale, flood basalt formations, such as the Deccan traps, may have been associated with SO_2 flux as high as a million kt/d estimated using the petrologic method, namely, the difference of volatile concentrations measured in nondegassed, phenocryst-hosted melt inclusions, and those in degassed groundmass glass scaled to the mass of erupted magma [*Self et al.*, 2006; *Devine et al.*, 1984].

Estimation of the total mass of SO_2 released during an eruption is not straightforward and often requires combination of various methods, such as the petrologic method and the remote sensing of SO_2 emissions. It also requires robust evaluation of the different techniques in order to avoid potential pitfalls. Regarding the

petrologic method, complications arise from the fact that sulfur in volcanic emissions may derive from different sources: "primary" sulfur initially dissolved in the degassing magma, "secondary" sulfur released by the breakdown of S-bearing minerals (usually sulfides), and "external" sulfur present in a coexisting gas phase at depth [e.g., *Scaillet et al.*, 2003]. The petrologic method must also accommodate the potential effects of sulfide saturation, sulfide magma separation, and/or sulfide destabilization (sink or source) on the total magmatic sulfur budget. Degassing budgets derived from remote sensing must also be carefully examined. Recent studies show that satellite-based estimates of volcanic SO_2 fluxes may widely vary depending on the type of sensors (IR or UV) and their radiometric capabilities (broadband or hyperspectral), in addition to temporal and spatial resolution imposed by the satellite orbit (geostationary orbit (GEO) versus low Earth orbit (LEO)) [e.g., *Thomas et al.*, 2009; *Theys et al.*, 2013]. Retrieval schemes (e.g., box, traverse, or delta-M methods) used for determination of SO_2 concentrations and fluxes from a given image may also lead to significantly different results as in the case of the 2010 Eyjafjallajökull eruption [*Carboni et al.*, 2012]. However, cautiously processed spaceborne measurements yield consistent results as demonstrated by *Corradini et al.* [2009], who obtained very similar volcanic SO_2 fluxes of 40 and 50 kt/d during the 24 November 2006 Mount Etna (Italy) eruption using Spinning Enhanced Visible and Infrared Imager (SEVIRI) and Moderate Resolution Imaging Spectroradiometer (MODIS) sensors, respectively. Finally, ground and space remote methods for sensing of SO_2 flux from erupting volcanoes may also give different results [e.g., *Beirle et al.*, 2014]. Nevertheless, determination of SO_2 fluxes using different methods should eventually lead to improved understanding of the methods themselves and, hence, the derived flux estimates.

The most common scheme for active volcanoes is that SO_2 fluxes measured by remote sensing techniques exceed by far those computed with the petrologic method. This is widely known as the so-called excess sulfur conundrum, recognized for several decades at arc volcanoes [e.g., *Luhr et al.*, 1984] and extensively reviewed elsewhere [e.g., *Scaillet et al.*, 2003; *Wallace*, 2005]. In contrast, during the sub-Plinian 2011 eruption at Grímsvötn volcano, Iceland, satellite measurements gave order of magnitude lower SO_2 atmospheric mass loading than that of the petrologic method, explained by multiple inventories of sulfur and important role of sulfides as a sulfur sink [*Sigmarsson et al.*, 2013].

Besides SO_2 and other major gases, volcanic emissions contribute to the atmospheric cycles of many trace elements [e.g., *Aiuppa et al.*, 2003] due to their enrichment in many alkali, alkali earth, transition, and heavy metals [e.g., *Zoller et al.*, 1974]. This volcanic input may have significant impact on the local environment by either polluting (e.g., toxic heavy metals) or fertilizing (e.g., alkali and alkali earth metals) terrestrial and aquatic ecosystems [e.g., *Frogner et al.*, 2001]. It is thus important to assess trace element fluxes by volcanic activity. Global flux estimates for most trace metals remain poorly constrained because of a rather limited number of studied volcanoes worldwide [*Allard et al.*, 2015]. In addition, since the pioneering work by *Lambert et al.* [1976], it is well known that volcanic gases and aerosols are significantly enriched in U series radioactive isotopes, namely, the radon daughters, ^{210}Pb, ^{210}Bi, and ^{210}Po. These isotopes are strongly fractionated upon degassing, leading to measurable radioactive disequilibria in volcanic exhalations [*Lambert et al.*, 1985]. Due to their radioactive properties and suitable half-lives, they can be used to set constraints on both shallow magma dynamics beneath active volcanoes and timescales of degassing processes [e.g., *Gauthier et al.*, 2000].

The 2014–2015 eruption at Holuhraun in the Bárðarbunga volcanic system in Iceland produced a great quantity of gas including sulfur dioxide. The SO_2 concentration frequently exceeded the health limit of 350 $\mu g/m^3$ with consequent influences on daily life for habitants closest to the eruption site [*Gíslason et al.*, 2015]. The extended duration of this basaltic fissure eruption (6 months from 29 August 2014 to 27 February 2015) led to considerable major volatile and trace metal fluxes to the atmosphere. It thus presents a rare occasion to study degassing processes at a volcano fed by a mantle plume. The SO_2 flux is quantified here with two different approaches: (i) a 3-month long, high-resolution time series of satellite data (Meteosat Second Generation (MSG)-SEVIRI) which are processed using an improved retrieval scheme based on the positive gradient method and (ii) the petrologic method based on the sulfur composition of melt inclusions within carefully selected phenocrysts, groundmass, and whole rock lava. Subsequent SO_2 fluxes are then deduced by scaling the sulfur degassing efficiency in Bárðarbunga magmas to the volume of erupted lavas. Despite the remote location of the eruption and sustained eruptive activity, a high-quality gas sample of the diluted plume could be collected. It was analyzed for major volatile species and trace element concentrations together with samples of tephra and lava. Their concentrations are scaled to the total SO_2 flux released during the entire eruption, in order to determine the atmospheric mass loading of both chalcophile (having a geochemical affinity for sulfur) and siderophile (having a

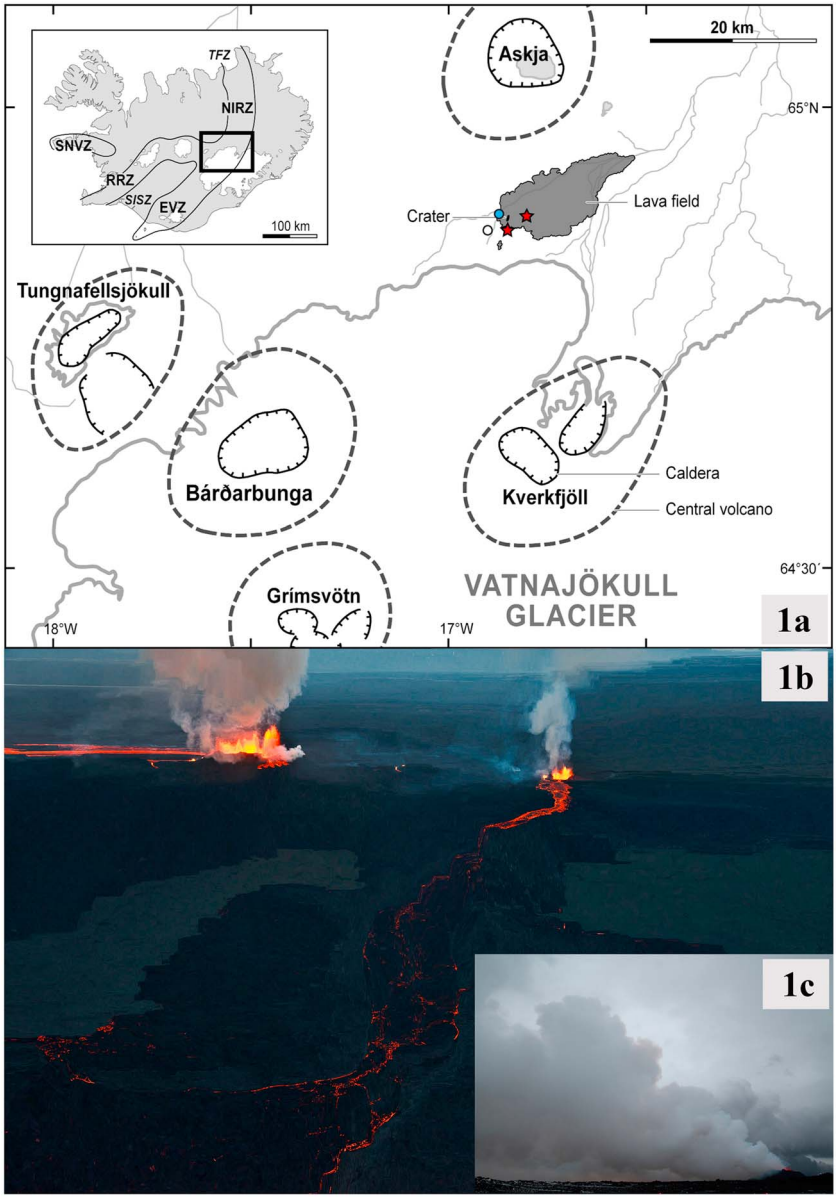

Figure 1. Simplified sketch map and pictures of the studied area. (a) Map showing the Holuhraun lava field ~45 km NE of the Bárðarbunga caldera. Central volcanoes affected by the 2014–2015 rifting event are also shown. Red stars and blue and white circles refer to the collection sites for lava samples, volcanic gas, and atmospheric background samples, respectively. Inset: The Neovolcanic zones of Iceland. (b) Picture of the eruption site as of 5 September 2014, showing intense degassing activity from the main craters and degassed magma overflow from the active craters feeding the lava field (Photo credit: Örvar Atli Þorgeirsson—Arctic Photo, Reykjavik). (c) Picture of the gas plume falling to the ground on 2 October 2014 (courtesy of Ármann Höskuldsson).

geochemical affinity for iron) elements. Results are compared with published values from Mount Etna and Stromboli [*Aiuppa et al.*, 2003; *Allard et al.*, 2000], which together with those of Kīlauea and Erta Ale [*Mather et al.*, 2012; *Zelenski et al.*, 2013] allows discussion about contrasting metal volatility from volcanoes in different tectonic settings. Finally, the shallow magma dynamics giving rise to the observed large SO_2 flux is discussed in the light of ^{210}Pb-^{210}Bi-^{210}Po short-lived radioactive disequilibria in the gas phase.

2. Geological Settings

Located in the highlands of Iceland, to the north of the Vatnajökull ice cap (Figure 1a), the Holuhraun lava field extends on the northern fissure swarm that cuts through the Bárðarbunga central volcano. Taken

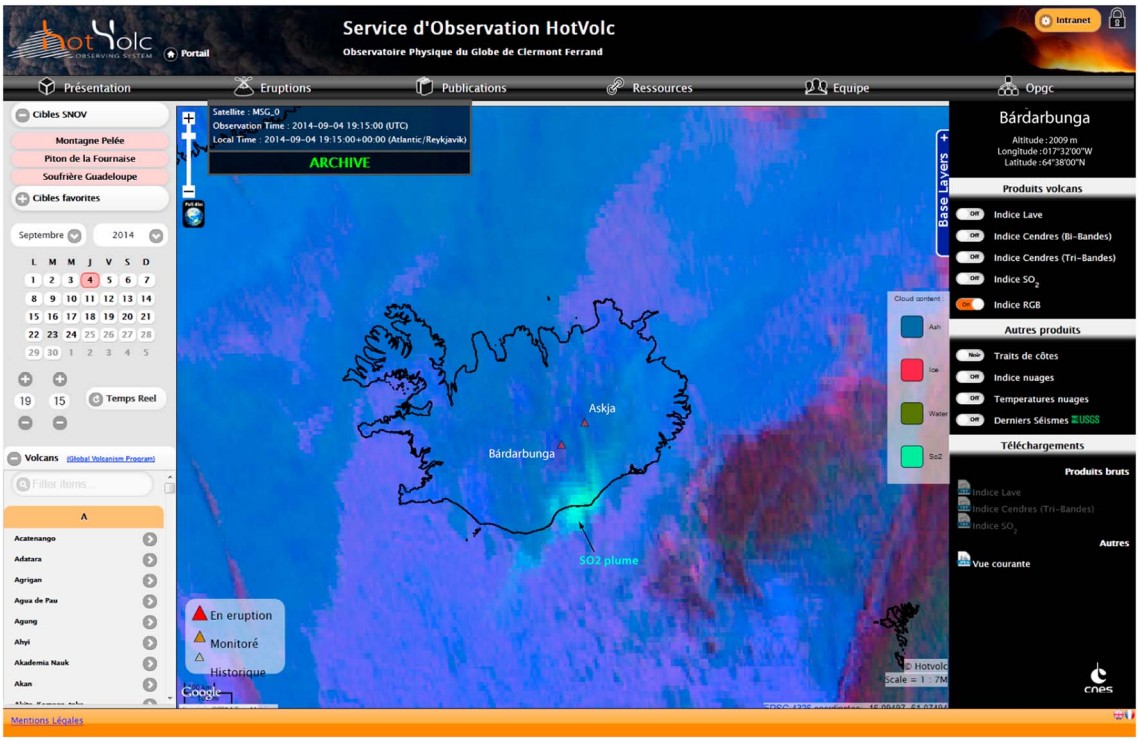

Figure 2. Snapshot of the HOTVOLC Web geographic information system user interface showing a large plume of SO_2 detected south of Holuhraun on 4 September 2014 at 19 h 15 UTC, using a RGB microphysics index (Red = 11–12 μm; Green = 12–8.7 μm; Blue = 11 μm).

together, the central volcano and its fissure swarms form an entity termed a volcanic system. This volcanic system sits on top of the Iceland mantle plume. Its southern fissure swarm has experienced the most volumetric basalt fissure eruption recorded during the Holocene. The Thjórsá lava field extends 130 km from central Iceland toward the south coast and into the North Atlantic, with a volume estimated close to 25 km^3 [*Hjartarson*, 1988]. During the Holocene, the Bárðarbunga volcanic system has produced olivine tholeiite basalts having restricted major element composition (MgO: 8–6%; K_2O: 0.1–0.3% [*Óladóttir et al.*, 2012, and references therein]). Historical eruptions have both produced lava fields and tephra from subglacial eruptions, last of which occurred at the end of 1902 [*Thorarinsson*, 1974].

As soon as 16 August 2014, an intense seismic swarm was detected underneath the NW of the Vatnajökull ice cap [*Gudmundsson et al.*, 2014; *Sigmundsson et al.*, 2015]. For the next 2 weeks, seismicity propagated from beneath the Bárðarbunga central volcano toward the north with associated ground deformation [*Sigmundsson et al.*, 2015]. On 29 August, the dyke intrusion ultimately triggered a brief, 4-hour long fissure eruption at the Holuhraun lava field, approximately 45 km NE of the central volcano (Figure 1a). Eruptive activity resumed in the morning of 31 August 2014, and the eruption lasted about 6 months until 27 February 2015. Lava fountaining initially occurred along a 1.5 km long eruptive fissure, with high magma discharge rates (approximately 250–300 m^3/s [*Gíslason et al.*, 2015]). By mid-September, the eruptive activity became limited to four main craters that grew until forming a 400 m long lava pond 2 months later. Lava production was accompanied by significant degassing activity at the main craters, generating a dense gas plume (Figure 1b). In contrast, magma overflowing the craters and feeding the lava field appeared almost entirely degassed and did not give rise to secondary gas plumes (Figure 1b), except when it flowed over water-saturated ground and the Jökulsá á Fjöllum riverbed. The volcanic plume rose almost vertically (Figure 1b), but under certain atmospheric conditions, the gas plume fell to the ground, thus giving unique opportunity to sample the primary magmatic gas released during the eruption (Figure 1c). Significant amounts of volcanic SO_2 were released during the first weeks of the eruption [*Gíslason et al.*, 2015; *Schmidt et al.*, 2015]. The sulfur dioxide was rapidly transformed to sulfuric acid that lead to acid rain and consequent rust formation on vehicles, plows, and other tools at farms nearby. When the eruption came to an end in late February 2015, the lava field covered 85 km^2 and its volume

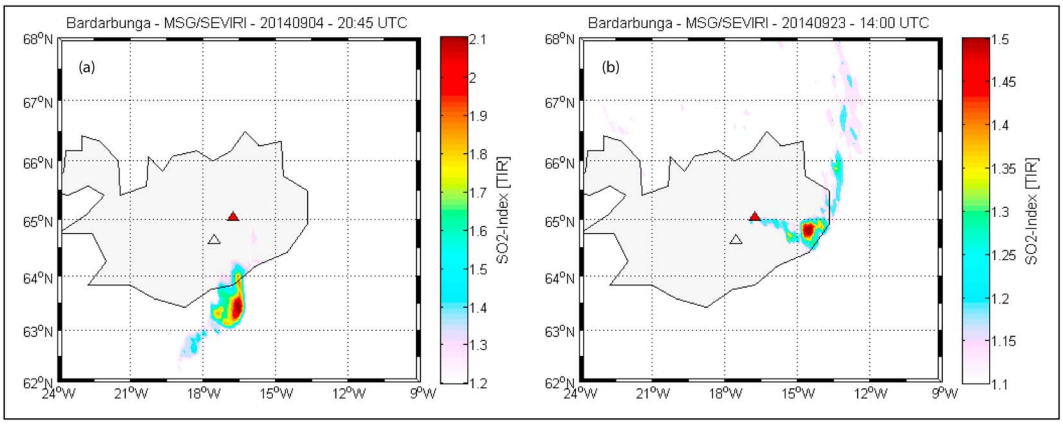

Figure 3. Maps of SO_2 plume (SO_2 index) during the Bárðarbunga eruption and detected by MSG-SEVIRI. White and red triangles show the locations of Bárðarbunga and Askja central volcanoes, respectively. (a) Plume of SO_2 disconnected from the vent, and drifting toward the south as detected on 4 September 2014 at 20:45 UTC. (b) Plume of SO_2 attached to the vent and drifting toward the east then toward the north, as detected on 23 September 2014 at 14:00 UTC.

was estimated at approximately 1.6 km^3 [*Gíslason et al.*, 2015], making it the largest eruption in Iceland for more than two centuries. Throughout the initial seismic crisis and the subsequent eruptive episode, no eruptive activity was observed at the Bárðarbunga central volcano itself. However, significant subsidence (up to ~50 cm/d) of the ice cap over the volcano was observed [*Sigmundsson et al.*, 2015]. It is most likely related to caldera collapse due to magma withdrawal at depth [*Riel et al.*, 2015].

3. Methods

3.1. Volcanic SO_2 Retrieval With Satellites

Satellite-based thermal infrared (TIR) data have now been used for more than two decades to derive the mass of volcanic SO_2 from maps of the total column abundance [*Realmuto et al.*, 1994] using absorption features of either the 8.7 μm wave band [e.g., *Watson et al.*, 2004] or the 7.3 μm wave band [*Prata et al.*, 2003].

In this study, we use TIR data from SEVIRI on board the geostationary (GEO) satellite named Meteosat Second Generation (MSG). Data come from the HOTVOLC remote sensing platform (see Figure 2) hosted by the OPGC (Observatoire de Physique du Globe de Clermont-Ferrand, France). Acquisition and processing of High Rate Information Transmission level 1.5 data format are made in real time through procedures explained in *Labazuy et al.* [2012]. Despite the satellite position at the intersection of the equator and prime meridian (longitude 0, latitude 0), MSG-SEVIRI fully covers the Icelandic region and can detect SO_2 plumes all over Iceland (Figures 3a and 3b). The technical capacity of both the satellite and the sensor itself can be found at the Eumetsat website http://www.eumetsat.int/website/home/Data/TechnicalDocuments/index.html

Various methods have been proposed to derive daily averaged SO_2 mass fluxes using low Earth orbiting satellite (LEO) data, such as the "box method" [*Lopez et al.*, 2013] or the "traverse method" [*Merucci et al.*, 2011], which are all based on the analysis of the SO_2 plume mass on a single or a few images. In contrast, MSG-SEVIRI routinely provides TIR data at the rate of one image every 15 min, allowing estimation of mass fluxes at much higher time resolution. However, the total mass of SO_2 cannot be simply estimated from the sum of the SO_2 plume mass retrieved from each image as significant overlap frequently exists between two successive images.

To address this issue, a method (named "positive gradient") has been developed specifically for the use of MSG-SEVIRI satellite for pulsed SO_2 plumes during long-lived effusive eruptions. The retrieval scheme comprises two main steps. First, the SO_2 column abundance is retrieved from the 8.7 μm wave band using a linear regression derived from a least square fitting procedure between sensor measurements and simulated radiances using the Modtran radiative transfer model [*Realmuto et al.*, 1994; *Corradini et al.*, 2009]. It leads to an instantaneous SO_2 mass in the gas plume. These calculations are made at each time step, yielding time

series of SO_2 mass erupted. Then, the SO_2 mass difference is calculated between each successive image (i.e., approximate derivative), leading to a time-averaged mass flux. This method is inspired by the "Delta_M" technique [e.g., *Krueger et al.*, 1996] using the mass conservation principle following the differential equation:

$$\frac{dM(t)}{dt} = \Phi(t) - kM(t) \quad (1)$$

In this equation, M is the mass of SO_2 contained in the plume on a given image at a given instant in time (t), dt stands for the time interval between two successive images, Φ is the input flux of volcanic SO_2, and kM is the output flux (i.e., SO_2 loss term). In the present case, observations were made close to the source vent, with a small time increment dt, leading to characteristic MSG-SEVIRI remotely sensed plume ages of approximately 5 h. Then, considering a typical SO_2 depletion rate between $2.8 \times 10^{-6} s^{-1}$ and $7 \times 10^{-7} s^{-1}$ [*Karagulian et al.*, 2010; *Krotkov et al.*, 2010; *Rose et al.*, 2003; *Lopez et al.*, 2013], the gas loss is estimated to be only in the range 1.3–5.2% of the total SO_2 burden, which is negligible. Similar conclusions were drawn from other studies using ground based [*McGonigle et al.*, 2004], Terra Advanced Spaceborne Thermal Emission and Reflection (ASTER) [*Urai*, 2004], and even Aura Ozone Monitoring Instrument (OMI) [*Lopez et al.*, 2013] measurements. The loss term can thus be deleted, and the discrete analytic solution of the time-averaged flux (Φ) can simply be written as

$$\Phi_{SO_2} = \frac{M_i - M_{i-1}}{\Delta t} \quad (2)$$

where i stands for the number of an image in the sequence. Importantly, the loss term being null, $dM/dt = 0$, means that the flux of SO_2 equals zero ($\Phi = 0$), and the plume is no longer fed by sulfur dioxide. Possible cases with $dM/dt < 0$ may be due to either dilution of the outer part of the plume to values below the detection limit of the sensor or to the incomplete plume coverage by the sensor field of view. These two situations are not likely to occur if the plume is continuously fed, when focusing on areas in vicinity of the source vent. Hence, in these specific conditions where the loss term is negligible, the quantity $dM/dt < 0$ indicates a theoretical interruption of the SO_2 mass flux and the positive mass difference only ($dM/dt > 0$) accounts for true SO_2 mass fluxes (thus the designation as the positive gradient method). At this stage, two different approaches can be used to calculate the total mass of SO_2 released during the eruption: first, from the discrete sum of products between SO_2 mass fluxes (Φ) and the time interval (Δt) for $dM/dt > 0$ such that

$$M_{tot} = \sum_{i=1}^{n} \Phi_{SO_2,i} \Delta t \qquad \text{for} \quad \frac{dM}{dt} > 0 \quad (3)$$

and second from the sum of peak values of instantaneous SO_2 mass measurements in the original time series. Both methods lead to exactly the same result.

Several limitations to the SO_2 retrieval procedure using infrared sensors may cause errors in SO_2 estimates. The accuracy depends mostly on the amount of gas, the plume altitude, the background surface temperature and emissivity, the water vapor, the water/ice clouds, and the instrument noise and specifications. Despite a strong SO_2 absorption cross section of the 7.3 μm wave band (~1×10^{-18} cm^2/molecule), low-altitude SO_2 plume, as in the present case (estimated visually on site in the range 1–3 km, 1–2 October 2014), cannot be detected due to the strong interaction with water vapor. Therefore, we used the 8.7 μm wave band, slightly less sensitive to SO_2 (~0.1×10^{-18} cm^2/molecule), but almost transparent to the water vapor, hence allowing SO_2 detection in the planetary boundary layer.

Over the Icelandic region, the sensor has a reasonably good spatial resolution with a mean pixel area of ~30 km^2. This is appropriate for near-vent records, but for distal portions of the plume, concentration of SO_2 may drop below the sensor detection limit. Also, at high satellite zenith angle, geometrical distortion, and mixing of radiance may affect measurements in the volcanic plume, leading to possible underestimation of the SO_2 burden. Distal records may also picture plumes with different ages, which necessitates taking into account the SO_2 depletion rate between two successive images. Nonetheless, geostationary satellites are capable of almost continuous monitoring (every 15 min using Meteosat-10), allowing SO_2 emissions to be pictured close to the source vent where their concentration can reach up to 100 DU (Dobson unit) or more (Figure 3b; see also Figure S1 in the supporting information). Issues related to plume dilution thus become less important for SO_2 fluxes calculated from regions close to the vent. The precision of SO_2 measurements in these conditions is estimated at ±10 DU for MSG-SEVIRI data [*Prata and Kerkmann,* 2007; *Eckhardt et al.*, 2008].

Table 1. Magnesium (Mg), Siderophile (Mo, W, and Re), and Chalcophile (Cu, Zn, As, Se, Ag, Cd, In, Sn, Sb, Te, Tl, Tb, and Bi) Trace Element Concentrations in Typical Chemical Blanks Obtained at Laboratoire Magmas et Volcans on Prewashed, Unexposed PTFE Membranes (Blank, From *Ménard et al.* [2014]), an Atmospheric Background Sample (BAR-Blk), Aerosol Filters (BAR-A and BAR-B), and Lava Samples (Average Values for Four Different Samples)[a]

				BAR-A (ng/m^3)	BAR-B (ng/m^3)	BAR-A (ng/m^3)	BAR-B (ng/m^3)					
	Lava ppm	Blank (ng)	BAR-Blk (ng/m^3)	(No Ash Correction)		(With Ash Correction)		EF (Mg) -	*D* -	ε (%)	(X/SO_2) (mg/kg SO_2)	Flux (kg/d)
Mg	42,000	nd	299	852	871	0	0	1	-	-	-	-
Cu	142	<ld	6.35	134	145	131	142	47.6	3.82×10^{-4}	2.69×10^{-4}	0.181	17.7
Zn	100	1.11	85.5	239	298	237	296	130	1.13×10^{-3}	7.97×10^{-4}	0.379	36.9
As	0.266	<ld	6.52	40.9	43.1	40.9	43.1	7.68×10^{3}	0.062	0.044	0.055	5.38
Se	*0.0142*	<ld	2.05	168	157	168	157	5.58×10^{5}	4.24	2.90	0.201	19.6
Mo	0.399	<ld	<ld	1.27	1.58	1.26	1.57	174	1.51×10^{-3}	1.07×10^{-3}	2.01×10^{-3}	0.20
Ag	0.282	nd	< ld	1.54	1.89	1.54	1.88	296	2.56×10^{-3}	1.80×10^{-3}	2.41×10^{-3}	0.23
Cd	0.232	<ld	0.29	330	390	330	390	7.57×10^{4}	0.65	0.45	0.499	48.7
In	0.082	< ld	0.01	6.74	7.73	6.74	7.73	4.30×10^{3}	0.036	0.026	0.010	0.96
Sn	0.987	0.0003	4.53	72.8	81.3	72.8	81.3	3.80×10^{3}	0.032	0.022	0.104	10.2
Sb	0.026	<ld	0.84	2.47	1.43	2.47	1.42	3.71×10^{3}	0.021	0.015	1.82×10^{-3}	0.18
Te	*0.00479*	0.001	0.32	158	178	158	178	1.71×10^{6}	14.3	9.15	0.228	22.3
W	0.093	<ld	<ld	0.075	0.1	0.073	0.098	46.0	4.08×10^{-4}	2.87×10^{-4}	1.26×10^{-4}	0.012
Re	0.002	nd	0.01	7.79	9.38	7.79	9.38	2.20×10^{5}	1.90	1.32	0.012	1.17
Tl	0.01	0.0001	0.05	6.07	5.83	6.07	5.83	2.94×10^{4}	0.23	0.16	7.46×10^{-3}	0.73
Pb	0.513	<ld	1.85	87.9	103	87.9	103	9.04×10^{3}	0.077	0.054	0.131	12.8
Bi	0.025	<ld	1.04	48	58.3	48	58.3	1.05×10^{5}	0.91	0.64	0.075	7.28

[a]"nd" stands for "not determined," "<ld" for "below detection limit." Selenium and Te concentrations in lava are estimated from their values in another Icelandic olivine tholeiitic basalt (BIR-1) [*König et al.* 2012]. Averaged enrichment factors relative to Mg (EF(Mg)) are calculated from data without ash correction. Averaged emanation coefficients (ε), liquid-gas partition coefficients (*D*), trace-to-SO_2 (X/SO_2) concentration ratios, and metal fluxes are calculated from data corrected for ash contribution.

The main source of error is likely due to the water/ice cloud cover that may prevent reliable measurements when it becomes optically thick. Therefore, we calculated a water/ice cloud cover index (%) simultaneously with the SO_2 retrieval, using the 11 μm wave band (surface cloud temperature) for the whole time series, at a rate of one image every 15 min. This index is used as a data quality flag within the HOTVOLC interface, and no correction is performed on the SO_2 measurements. The cloud cover varies from 5% to 100% but shows a net increase through time with an average cloud cover of 45% for September, 54% for October, and 61% for November. The cover becomes even more important during the winter period, preventing any reliable SO_2 measurements. Periods of low SO_2 detection could, in principle, be caused by large cloud coverage above the volcanic area, leading to underestimation of the actual SO_2 mass loading. This point will be further discussed in section 4.1.

3.2. Volcanic Gas and Lava Sampling and Analyses

3.2.1. Trace Element, Sulfate, and Halide Degassing

Major volatiles remain gaseous at the degassing vent, while trace elements are mostly born in the aerosol fraction of the plume, due to rapid gas-to-particle conversion upon quenching of the gas phase in the atmosphere [*Whitby*, 1978]. The volcanic gases and solid aerosols were collected on different strainers using filter packs during calm weather on 2 October 2014, to the west of the active lava craters (Figure 1a). Filter packs were composed of three filters in series. A Sterlitech® polytetrafluoroethylene (PTFE) laminated membrane filter, prewashed with dilute HCl, to collect the particulate phase (diameter: 47 mm and pore size: 1 μm), followed by two Whatman® filters previously impregnated with a mixture of 10% glycerol–10% $NaHCO_3$ to trap major gaseous species (SO_2, HF, and HCl [*Allen et al.*, 2000]). Each filter pack was connected to a pump having a pumping speed of 11 L/min. Two samples (BAR-A and BAR-B, Table 1) were collected during 1 h and 30 min, for a total volume of filtered air of 0.66 and 0.33 m^3, respectively. An additional sample (BAR-Blk) was collected away from the plume for 1 h in order to monitor the atmospheric background close to the eruption site. Sampling site locations can be seen in Figure 1a. In the laboratory, PTFE filters were first leached in 5 mL of dilute mixed solution of 0.4 M HNO_3 and 0.05 M HF for 1 week at moderate temperature (~90°C). The solutions obtained were then analyzed by inductively coupled plasma mass spectrometry (ICP-MS) at the Laboratoire Magmas et Volcans (LMV) in Clermont-Ferrand. Solutions were introduced directly into a quadrupole ICP-MS (Agilent 7500) for trace element concentration measurement. The reaction cell (in He mode)

was used to reduce interferences on masses ranging from Sc (45) to As (75), and the signal was calibrated externally against a standard solution. The 2σ reproducibility is close to 10%. The impregnated filters were leached with 20 mL of deionized water at ambient temperature. After 2 weeks, a few drops of H_2O_2 were added to the leachate in order to convert all S species into sulfates (SO_4^{2-}). The leachate was then diluted for analyses of sulfate and halide (Cl^- and F^-) concentrations by ion chromatography (Dionex ICS-1500) at the Institut de Chimie in Clermont-Ferrand. The associated errors (2σ) are approximately 2% for SO_4^{2-} and 10% for both F^- and Cl^- concentrations.

3.2.2. Radioactive Disequilibria of ^{210}Pb-^{210}Bi-^{210}Po in Volcanic Gas

Short-lived radionuclides, produced after the decay of radon in the ^{238}U chain, are strongly fractionated in volcanic gas and reveal large disequilibria between their activities [e.g., *Lambert et al.*, 1985; *Gauthier et al.*, 2000, and references therein]. These disequilibria are caused by the different volatility of radon daughters, and in basaltic magma the volatility of ^{210}Pb, ^{210}Bi, and ^{210}Po is estimated to be close to 1%, 10%, and 100%, respectively. The state of disequilibrium can be studied for approximately 5 times the half-life of the daughter nuclide and, thus, on different time scales due to variable half-lives of these radionuclides (22.3 years, 5.0 days, and 138.4 days, respectively). This implies, for instance, that ^{210}Bi-^{210}Pb disequilibria in volcanic gases can only be measured within the first month following the sampling.

Radionuclides in the gas phase were collected with a single-stage filter pack. The diluted plume was pumped through Poelmann-Schneider cellulose raw filter (diameter: 56 mm and pore size: 0.2 μm) over 1 h at a flow rate of 5.1 m^3/h (sample BAR-PS). The long sampling time was deemed necessary due to expected low radioactivity in the gas phase as inferred from low U and Th concentrations in earlier analyzed lava (Table S1). The filters were rapidly brought to LMV where the total α and β radioactivity was measured with a low-background $\alpha-\beta$ nuclear counting unit (Canberra IN20). Detailed results are given in Table S2. In practice, polonium is the only chemical element having α emitter isotopes to be volatile at magma temperature. Because most of these have negligible half-lives, gross α counting yields the ^{210}Po activity. Regarding β emitters, ^{210}Pb and ^{210}Bi are the only isotopes to be present on a filter as other lead and bismuth isotopes have too short half-lives (<30 min). Furthermore, the β decay energy of ^{210}Pb is too weak (17 keV) to be detected by the counting unit so that gross β counting gives a direct measurement of the ^{210}Bi activity. The ^{210}Pb activity is then determined through that of ^{210}Bi, 1 month after sampling when both isotopes have reached radioactive equilibrium. The 2σ errors on activities depend on counting statistics and, in the present case, average at 10% for both α and β emitters.

3.2.3. Melt Inclusions and Whole Rocks

The so-called petrologic method [*Devine et al.*, 1984] is based on the difference (ΔS) between sulfur concentrations measured in phenocryst-hosted melt inclusions (MI), taken to indicate the pre-eruptive concentration, and the outgassed groundmass glass representing the residual sulfur concentrations not emitted to the atmosphere. This difference, when scaled to the mass of magma erupted, yields the exsolved mass of sulfur. Magma degassing during basaltic fissure eruptions primarily occurs at the vents but considerable sulfur degassing takes place during the lava emplacement [e.g., *Thordarson et al.*, 1996]. Therefore, sulfur concentration measured in the lava better represents the "residual" concentration. For eruptions of known duration the average SO_2 flux is then readily calculated and the total mass of SO_2 emission when the erupted mass is known.

Lava, fresh tephra, and Pele's tear samples were collected during the first months of the eruption at Holuhraun (Figure 1a). Clinopyroxene and plagioclase crystals were handpicked under a binocular microscope from the 250–500 μm grain size fractions. Crystals with melt inclusions were washed with acetone, embedded in epoxy, and polished individually to generate adequate exposure of the MI for in situ electron probe microanalysis. Major element and volatile concentrations were measured on a Cameca SX-100 microprobe at LMV. The results are given in Table S3, and analytical details and uncertainties are listed in *Óladóttir et al.* [2011] and *Moune et al.* [2012]. The largest MIs were analyzed with a spot diameter of 20 μm and a sample current of 8 nA, whereas the three smallest MIs were analyzed with a beam of only 5 μm and a current as low as 4 nA.

Whole rock major and trace element concentrations were determined in solutions at LMV by ICP atomic emission spectroscopy and quadrupole mass spectrometry (ICP-MS) using published methods [e.g., *Sigmarsson et al.*, 2011]. Total sulfur concentration on the holocrystalline lava was measured with a Thermo Fisher CHNS/O analyzer at LMV. Approximately 20 mg of dried and finely powdered basalt are mixed with 10 mg of vanadium oxide and combusted under oxygen and helium flow at 1800°C. Sulfur plus oxygen form sulfur dioxide and trioxide that are consequently transformed to SO_2 by passage through copper oxide reaction cell

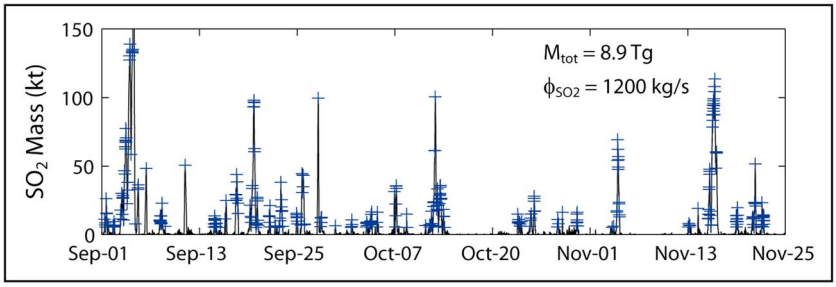

Figure 4. Time series of the sulfur dioxide mass (in kilotons) for the first 3 months (1 September 2014 to 25 November 2014) of the eruption at Holuhraun. Blue symbols indicate the peak values selected for the calculation of the SO_2 mass fluxes (see text for details). This sums up to a total SO_2 mass of 8.9 ± 0.3 Tg and a SO_2 mass flux of 1200 ± 40 kg/s.

before the signal detection. The instrument is calibrated with an organic analytical standard, 2,5-Bis(5-tert-butyl-benzoxazol-2-yl)-thiophene and the sulfur analytical accuracy is determined from measurements of a reference material, *Soil*, calibrated against Acetanilide 141d from the National Institute of Standards and Technology, Maryland, USA. Seven analyses of Soil yield S = 0.029 wt% ± 0.005 (2 SD) but results are reported in Table S3 relative to the certified Soil value of 0.023 wt%.

4. Results

4.1. Volcanic SO_2 Estimate

Images from MSG-SEVIRI for 1 September to 25 November (86 days in total) were processed at a time resolution of one image every 15 min, which totals 8256 images. Unfavorable weather conditions from late November 2014 to March 2015 rendered satellite observations fragmented and, thus, imprecise. Two maps of the SO_2 plume are shown in Figure 3. The detection is made using the radiance difference ($Wm^{-2}\,sr^{-1}\,\mu m^{-1}$) between wave bands at 11 μm and 8.7 μm and displayed as a SO_2 index. During clear-sky conditions, SO_2 can be detected from a SO_2 index threshold of ~1.2 and can reach maximum values higher than 2. Figure 3a shows the SO_2 plume on 4 September 2014 (20:45 UTC), drifting toward the south and disconnected from the vent. It suggests that the plume is not fed uniformly, causing transient SO_2 degassing. A maximum SO_2 index of 2.32 was reached on this day, characterized by excellent weather conditions and limited cloud cover of only ~10%. In contrast, Figure 3b shows a SO_2 plume on 23 September 2014 (14:00 UTC) drifting toward the east and then to the north. Despite less favorable conditions (>20% cloud coverage), the MSG-SEVIRI still allows accurate detection of SO_2 with the SO_2 index reaching 1.68. In this latter case, the SO_2 plume is connected to the vent with a continuous lace of SO_2 over hundreds of kilometers.

The time series in Figure 4 reveals the first SO_2 emission peaks between 3 and 5 September, shortly after the onset of the eruption. The maximum instantaneous SO_2 mass is equal to 226 kt on 5 September at midnight. A similar pattern can be seen from both OMI and IASI sensors [*Schmidt et al.*, 2015] although the maximum SO_2 burden quoted by these authors reaches only 170–180 kt. The higher value measured using MSG-SEVIRI is ascribed to better time resolution and imaging of the very onset of this large degassing activity. A prodigious time-averaged SO_2 flux of ~4000 kg/s is obtained for the first days of the eruption. After the initial phase of the eruption, the instantaneous SO_2 mass decreases and typically varies from 25 kt to 100 kt yielding time-averaged SO_2 flux of ~900 kg/s. The lowest SO_2 discharges are probably not caused by a higher cloud coverage preventing quantitative observation of the plume. The SO_2 was indeed accurately detected on cloudy days such as 23 September 2014 (Figure 3b) and in mid-November under a significant cloud cover (SO_2 up to 96 kt with a cloud mask of 41%), while weak SO_2 emissions were recorded even during clear-sky conditions at the end of October ($SO_2 < 1$ kt with a cloud cover of only 8%). Although our estimate of the SO_2 burden must be regarded as a minimum value because of potential cloud obscuration, it suggests that reliable SO_2 retrieval through MSG-SEVIRI images is still possible when the cloud cover remains below a reasonable value, estimated at ~50%. These results also suggest a pulsating nature of the SO_2 emissions from this eruption. Overall, the total SO_2 mass released by the Bárðarbunga volcanic system during the first 3 months of the eruption amounts to 8.9 ± 0.3 Tg, which leads to a mean SO_2 mass flux of 1200 ± 40 kg/s (equivalent to an average of 104 ± 4 kt/d). This 3 month average is indistinguishable from the OMI-derived

Table 2. Sulfur, Chlorine, and Fluorine Contents in Volcanic Gases (Samples BAR-A and BAR-B), Undegassed Magma Trapped in Melt Inclusions (MI) and Degassed Products (Degassed Lava (DL) or Glassy Groundmass (GG))[a]

	Gas geochemistry			Petrology		
Chemical Elements	BAR-A (mg/m^3)	BAR-B (mg/m^3)	Chemical Elements	MI (ppm)	DL or GG (ppm)	Δ (ppm)
SO_2	369	781	S	1407	97 (DL)	1310
HCl	3.64	10.0	Cl	73	49 (GG)	24
HF	0.50	0.71	F	<ld	<ld	nd
S/Cl	52	40	S/Cl (from petrology = ΔS/ΔCl)			55
Cl/F	7.5	14	nd			nd

[a]Δ is the degassing yield for volatile species, calculated from the difference between the initial volatile content preserved in melt inclusions minus the residual volatile content in degassed products (see text for further explanation). "<ld" stands for "below detection limit" and "nd" stands for "not determined".

SO_2 flux of 99 kt/d in September [*Schmidt et al.*, 2015]. Further comparison can be made with differential optical absorption spectroscopy (DOAS) ground measurements [*Gíslason et al.*, 2015]. Our SO_2 flux estimate is in good agreement with, although slightly lower than, that measured by DOAS during the first weeks of the eruption (1380 kg/s), which is best explained by the relative importance of the initial degassing event for different time windows. This initial degassing exceeds the SO_2 flux measured in December 2014 to January 2015 (~550 kg/s) by a factor of 2.2. This lower value suggests a gradual decline in gas emissions, associated with a significant decrease in the lava effusion rate [*Gíslason et al.*, 2015] after November 2014 until the end of the eruption on 27 February 2015.

Compared to other active hot spot-related volcanoes, the SO_2 flux measured at Holuhraun appears considerably greater. It is for instance 4 to 10 times higher than the current SO_2 flux measured at 100–250 kg/s at Kīlauea, Hawai'i [*Beirle et al.*, 2014]. It is up to 3 orders of magnitude more important than the 1.3 kg/s measured from the passively degassing lava lake of Erta Ale, Ethiopia [*Oppenheimer et al.*, 2004]. The magnitude of the continuous degassing of SO_2 during the eruption at Holuhraun actually resembles the SO_2 flux released during sudden short-lived eruptions like at Piton de la Fournaise, Reunion Island [*Gouhier and Coppola*, 2011] or Sierra Negra, Galapagos [*Thomas et al.*, 2009], with the noticeable difference that the eruption at Holuhraun lasted for 6 months. Besides hot spot volcanoes, even Etna volcano (Sicily), one of the world largest contributors of volcanic SO_2 to the atmosphere [e.g., *Allard*, 1997], produces maximum SO_2 fluxes reaching only one fourth of the SO_2 discharge from the Holuhraun eruptive fissure. Taken together, the SO_2 flux from the Bárðarbunga volcanic system is the largest measured so far for basaltic fissure eruptions.

4.2. Volcanic Gas

4.2.1. Major Gas Species

The diluted plume of Holuhraun is characterized by high concentrations of major gases with SO_2, HCl, and HF, respectively, in the range 369–781, 3.6–10, and 0.5–0.7 (in mg/m^3; Table 1). These concentrations are much higher than the atmospheric background in Iceland [*Moune et al.*, 2006], which can thus be neglected. Significantly lower concentrations in sample BAR-A compared to BAR-B strongly suggest that impregnated filters became saturated with major gas species before the end of the 1 h long sampling. The saturation capacity of $NaHCO_3$ impregnated filters is not accurately known, but the present results suggest it could be significantly higher than previously thought [*Mather et al.*, 2008]. The two samples have nevertheless S/Cl within analytical errors suggesting that sulfur dioxide and halogen gases contemporaneously reached saturation in sample BAR-A. The mass ratios between volatile elements in the filter samples represent those in the eruptive gas phase. The S/Cl and Cl/F are in the range 40–52 and 7.5–14, respectively, which compares well with observations from other hot spot volcanoes like Erta Ale, Ethiopia (S/Cl ~ 21, Cl/F ~ 3 [*Zelenski et al.*, 2013]) or Kīlauea, Hawai'i (S/Cl ~ 40–85, Cl/F ~ 2 [*Symonds et al.*, 1994; *Edmonds et al.*, 2013]). These ratios reveal very low Cl and even lower F degassing at Holuhraun, as well as at other mantle plume-related volcanoes.

4.2.2. Trace Elements

The trace element analyses of the leached filters (Table 1 and Table S1) are the first results ever published for an eruptive volcanic gas plume released during an eruption in Iceland. A special emphasis is given here to both siderophile and chalcophile elements which usually are the most enriched trace elements in volcanic gases [e.g., *Zelenski et al.*, 2013]. Concentrations in the diluted plume range from 0.1 ng/m^3 for W to 400 ng/m^3 for Cd (Table 1).

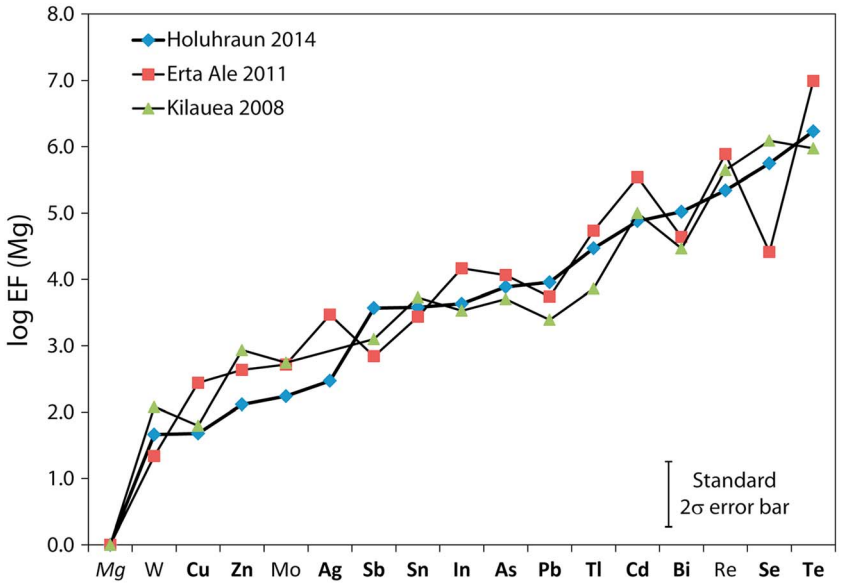

Figure 5. Trace element volatility expressed as enrichment factors relative to Mg (EF) for Holuhraun and gas plumes from Kīlauea (EF recalculated to Mg from *Mather et al.* [2012]) and Erta Ale [*Zelenski et al.*, 2013]. Trace elements are ranked according to their order of increasing volatility at Holuhraun. Siderophile and chalcophile elements are shown in light and bold characters, respectively.

Volcanic aerosols are collected with other solid particles (e.g., tephra) on the PTFE membranes by filtration of the diluted plume. On such filter samples, trace element concentrations $[X]_P$ are thus given by the relation

$$[X]_P = d[X]_G + (1-d)[X]_A + a[X]_{Sil} \quad (4)$$

where brackets denote concentrations of an element X and subscripts P, G, A, and Sil refer to diluted plume, magmatic gas, atmospheric background, and silicate material (i.e., ejected tephra, dust remobilized by wind, and silicate spherules), respectively. The "d" represents proportion of magmatic gas diluted in the atmosphere, and "a" stands for the amount of silicate material collected on the membrane. For most of the trace elements, concentrations in the atmospheric background (BAR-Blk, Table 1) account for less than 5% of overall concentrations in the volcanic plume and are neglected accordingly. However, this contribution reaches 15% for As and up to 35% for Mg, Zn, and Sb. Standard atmosphere over Iceland is free of significant trace pollutants [*Moune et al.*, 2006], so that these high background values are thought to arise from an artifact and are not further considered. The amount of silicate material collected on filter samples usually is determined from the concentration of the least volatile trace elements [*Gauthier and Le Cloarec*, 1998; *Aiuppa et al.*, 2003]. Very low rare earth element and Th concentrations in our samples (Table S1) suggest negligible amounts of ash (about 10 μg of ash per filter on average). Accordingly, the ash contribution for all volatile elements can be neglected and we consider here that volatile trace element abundances in the plume only reflect their primary degassing at magmatic temperature.

Trace element volatility is often expressed relative to a reference element R by means of an enrichment factor defined as

$$\mathrm{EF}(X) = \frac{[X]_P/[X]_L}{[R]_P/[R]_L} \quad (5)$$

where subscripts P and L refer to the concentration of a given trace element X or R in the volcanic plume and the lava, respectively. The choice of a reference element is critical when dust or ash is collected together with the aerosol during windy conditions (see Text S1). Enrichment factors (EF) relative to Mg are calculated from trace element concentrations in the two plume samples and the average lava composition (Table 1). Enrichment factors are given in Table 1 and shown in Figure 5. All chalcophile and siderophile elements appear moderately to highly volatile in the Holuhraun plume. The least volatile elements W, Cu, Zn, Mo, and Ag have EF in the range 50–300. In contrast, Cd, Bi, Re, Se, and Te appear to be extremely volatile with EF reaching 10^5–10^6. This trend relies only on two high-quality samples of primary magmatic gases and aerosols. However, gas composition did not vary much after the very first degassing event in early September

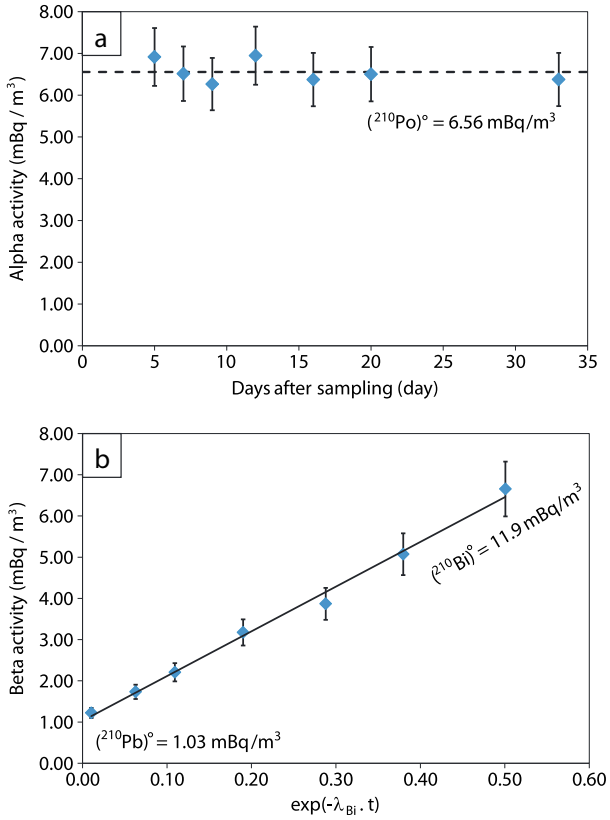

Figure 6. (a) Time evolution (in days after sampling) of alpha activities in an aerosol filter (sample BAR-PS). Constant activities through time allows the determination of the initial $(^{210}Po)_0$ activity in the gas plume at 6.56 ± 0.27 mBq/m^3; (b) time evolution (expressed as $\exp(-\lambda_{Bi} \cdot t)$, where λ_{Bi} is the decay constant of ^{210}Bi and t represents the number of days after sampling) of beta activities in sample BAR-PS. Beta activities linearly decrease with time according to ^{210}Bi half-life, thus allowing the determination of initial $(^{210}Pb)_0$ and $(^{210}Bi)_0$ activities in the gas plume equal to 1.03 ± 0.10 mBq/m^3 and 11.9 ± 1.3 mBq/m^3, respectively (see text for further explanation).

[*Gíslason et al.*, 2015] allowing considering these two samples as representative of the gas composition throughout the eruption. These results are compared in Figure 5 to trace element gas data from other mantle plume-related volcanoes, namely, Kīlauea, Hawai'i [*Mather et al.*, 2012] (their initial EFs relative to Al have been recalculated to Mg) and Erta Ale, Ethiopia [*Zelenski et al.*, 2013]. Despite minor differences on EF values between the three volcanoes (less than 0.7 log unit on average), a consistent overall degassing pattern is observed for the three mantle plume-related volcanoes. The strongest variations in EF are observed for both Se and Te, which in part may be due to analytical difficulties in determining their concentrations in the lavas. Despite these small differences, a singular mode of metal degassing seems to occur at all these three hot spot volcanoes.

4.2.3. Short-Lived Radioactive Disequilibria

Both α and β activities were repeatedly measured over approximately a month after sampling, the time necessary to reach radioactive equilibrium between ^{210}Bi and ^{210}Pb. The activities measured on the filters are the lowest ever measured by α- and β-counting techniques in our laboratory. The background of all the detectors was characterized specifically for each step of the counting process and subsequently subtracted from the measurements. Due to relatively long half-life of ^{210}Po (138.4 days), its activity remained constant during the (^{210}Bi) measurements (Table S2 and Figure 6a). The $(^{210}Po)_0$ activity at the time of gas sampling was 6.56 ± 0.27 mBq/m^3. In contrast, decreasing (^{210}Bi) activity during the measurements is explained by its relatively short 5 day period. Figure 6b shows the linear decrease of (^{210}Bi) with time that allows determination of both $(^{210}Pb)_0$ at $t > 30$ days and $(^{210}Bi)_0$ at $t = 0$. This yields $(^{210}Bi)_0 = 11.9 \pm 1.3$ mBq/m^3 and $(^{210}Pb)_0 = 1.03 \pm 0.10$ mBq/m^3 at the time of sampling.

The volcanic plume of Holuhraun is thus characterized by $(^{210}Bi/^{210}Pb)_0$ and $(^{210}Po/^{210}Pb)_0$ of 11.5 and 6.4, respectively. The former ratio is close to $(^{210}Bi/^{210}Pb)_0$ ratios measured at other basaltic systems like Etna [*Lambert et al.*, 1985] or Stromboli [*Gauthier et al.*, 2000] or even at volcanoes producing more differentiated magma like Merapi, Indonesia [*Le Cloarec and Gauthier*, 2003]. The isotopic signature of the Holuhraun gas thus appears to be characteristic of a primary magmatic vapor rapidly released from an active magma batch, which is continuously replenished [*Gauthier et al.*, 2000]. In contrast, the $(^{210}Po/^{210}Pb)_0$ is 1 order of magnitude lower than commonly found elsewhere. This could be tentatively explained by a much lower volatility of polonium at hot spot volcanoes compared to the case of subduction-related volcanoes. However, both Se and Te are extremely volatile at Holuhraun (Table 1) and all elements of the S-Se-Te-Po column of the periodic table are expected to behave similarly. Thus, this hypothesis is considered unlikely. Furthermore, polonium is extensively degassed at the Loihi seamount in Hawai'i [*Rubin*, 1997, and references therein] and in basalts of

the Eyjafjallajökull flank eruption [*Sigmarsson et al.*, 2015]. Low $(^{210}Po/^{210}Pb)_0$ activity ratio at Holuhraun is thus best explained by former ^{210}Po depletion (further discussed in section 5.4) prior to shallow degassing beneath the eruptive fissure.

4.3. Melt Inclusions

The MI are spherical to oblate in shape and range in size from 15 to 65 μm. Most MI contain shrinkage bubbles, but all are completely free of daughter minerals. In total, 14 crystals containing 20 MI were selected for analysis. The number of host crystals with MI reflects the relative abundance in the phenocryst assemblage; 16 MI in 11 plag and 4 in 3 cpx. The tephra and earliest lava groundmass is composed of glass patches with variable crystallinity, whereas that of channel-fed lava is holocrystalline.

All MI are of olivine tholeiitic composition. Sulfur concentrations in the MI vary from 932 to 1591 ppm (Table S3), whereas lower values are measured in the groundmass glass (GG) of Pele's tears (308 to 469 ppm; mean = 389 ± 23 ppm; 2 SE on 14 glass grains). The total sulfur of the degassed lava (DL) is even lower or 97 ± 10 ppm (2 SE; five analyses). Correlation between S and MgO concentrations of the MI strongly suggests negligible host crystallization at the expense of the MI (Figure S2). The S concentrations in the MI plot close to the sulfide saturation curve of submarine mid-ocean ridge basalt glasses [e.g., *Wallace and Edmonds*, 2011] in accordance with the presence of sulfide globules in the groundmass (Figure S3). Sulfide saturation and known sulfur content at sulfide saturation level in basalts [e.g., *Jugo et al.*, 2010] suggest that the Bárðarbunga 2014 magma has oxygen fugacity close to the fayalite-magnetite-quartz (FMQ) buffer (Figure S3). This concurs with fO_2 estimates of 0 to 1 log unit above the FMQ buffer based on the Kα ray position of sulfur [*Carroll and Rutherford*, 1988].

The electron microprobe volatile analyses of the MI yield fluorine concentration below the detection limits. Chlorine concentrations are also low, only reaching values as high as 178 ppm. They have indistinguishable average values between the groundmass glasses (range: 49–141 ppm; mean: 93 ppm ± 23 ppm (SD)) and the MI (range: 54–178 ppm; mean: 96 ppm ± 40 ppm (SD)). The pre-eruptive volatile concentrations are estimated from the average concentrations in the clinopyroxene-hosted MI, which have been shown to represent the juvenile composition of magma elsewhere in Iceland [*Sigmarsson et al.*, 2013].

Like for sulfur, the lowest Cl concentrations are expected to be found in the degassed lava sample (DL). In the absence of such data, it is assumed that the lowest Cl concentration measured in the tephra groundmass glass represents the final residual content. This allows a crude estimate of potential chlorine degassing, and hence determination of the maximum S/Cl of the gas phase which is calculated from the following ratio: $(S_{MI} - S_{DL})/(Cl_{MI} - Cl_{GG})$. It yields (1407 ppm − 97 ppm)/(73 ppm − 49 ppm) = 55, in good agreement with the ratio measured in the gas phase (Table 2). In the event that Cl had degassed even more than estimated here, the theoretical S/Cl calculated from the petrologic method would be lower and match even better the measured gas ratios. This observation supports concurrent shallow degassing of Cl and S beneath the Holuhraun site.

4.4. Sulfur Dioxide Fluxes From Melt Inclusions

Hydrogen sulfide (H_2S) concentrations above the olfactive threshold were reported in Scandinavia and attributed to gas emissions from Holuhraun [*Grahn et al.*, 2015]. However, MultiGAS monitoring of primary magmatic vapors at the eruption site did not reveal significant amounts of H_2S [*Gíslason et al.*, 2015], which suggests that H_2S concentrations were probably less than a few percent of the total S budget, like at other hot spot-related volcanoes [*Symonds et al.*, 1994; *Zelenski et al.*, 2013]. We thus assume that all sulfur lost from the magma was degassed as SO_2. The mass of degassed SO_2 is calculated by the petrologic method according to

$$\text{Mass of } SO_2 = M(SO_2)/M(S) \times \rho_{melt} \times (1 - \varphi) \times V_{lava} \times \Delta S \quad (6)$$

where the ratio of molar masses M is equal to 2, ρ_{melt} is the density of the melt calculated at 2750 kg/m^3, ΔS is the sulfur yield calculated as explained above ($S_{MI} - S_{DL} = 1310$ ppm), φ is the void proportions in the lava, which is visually estimated at 10% (estimated error of 30%), and V_{lava} is the volume of erupted lava (km^3). Note that the crystal fraction is neglected in equation (6) since the analyzed Holuhraun lavas are phenocryst poor. The lava volume was estimated at 1.6 ± 0.3 km^3 [*Gíslason et al.*, 2015]. It yields a total mass of SO_2 of 10.4 ± 1.9 Tg released over 180 days, corresponding to an average SO_2 flux of about 57 kt/d or 670 kg/s, in good agreement with DOAS-derived average SO_2 fluxes for the entire eruption [*Gíslason et al.*, 2015]. Similarly,

the volume of erupted lava was estimated at 1.2 km^3 from time series satellite measurements after 86 days of eruption at the end of November 2014 [*Gouhier et al.*, 2015, 2016]. The mass of SO_2 released during the first 3 months is thus estimated from the petrologic method at 7.8 ± 1.5 Tg. It corresponds to an average flux of approximately 90 kt/d or 1050 kg/s, in good agreement again with the SEVIRI-derived SO_2 fluxes for the same period. This suggests that all degassing magma at depth contributed to the lava eruption and the gas plume.

5. Discussion

5.1. Large Sulfur Dioxide Flux

Quantification of SO_2 fluxes from an active volcano is not trivial. Both the petrologic method and the satellite measurements suffer from difficult-to-quantify approximations. The former method relies upon identification of the pre-eruptive and final sulfur concentrations in the erupted magma as well as the accurate quantification of erupted volumes. For the latter method, satellite measurements may be conditioned not only by the weather conditions but also by many other parameters such as the amount of ash or the sulfur speciation in the eruptive gas plume. Ideally, both approaches should converge to a similar value. However, atmospheric mass loading of sulfur, estimated from melt inclusion studies, has been compared with satellite analyses and most of the time the latter method has shown excess sulfur [e.g., *Wallace*, 2005]. This is especially true for volcanoes at subduction zones, whereas both methods appear to concur to similar values for basaltic eruptions at hot spot volcanoes [*Sharma et al.*, 2004]. Two recent eruptions in Iceland, namely, the 2000 Hekla and 2011 Grímsvötn eruptions [e.g., *Moune et al.*, 2007; *Sigmarsson et al.*, 2013] showed higher SO_2 estimated with the petrologic method than measured by remote sensing. In the first case, the eruption took place during wintertime with loss of SO_2 signal to the satellites caused by ice formation in the eruption plume [*Rose et al.*, 2006]. This illustrates how it may be difficult to properly estimate the atmospheric sulfur mass loading for explosive eruptions during bad weather conditions. In the second case, sulfide saturation in tholeiitic basalt magma led to mismatch between the remote sensing and the petrologic method by a factor of 2. The sulfides may act as a source for sulfur or a sink. In the first case, sulfides may be destabilized during degassing and oxidation, which would lead to underestimation of sulfide dioxide mass loading calculated by the petrologic method relative to the satellite-based calculation. In the second case, the sulfide may act as a sink as was observed for the 2011 Grímsvötn eruption [*Sigmarsson et al.*, 2013]. The role of the scarce sulfides in the groundmass of the lava erupted at Holuhraun appears to be minimal. The eruption at Holuhraun thus follows the general trend for hot spot volcanoes with similar fluxes estimated with the satellite and the petrologic methods.

With an average SO_2 flux of about 1130 kg/s for the three first months of the eruption (mean value obtained from SEVIRI measurements at ~1200 kg/s and the petrologic method at ~1050 kg/s), the SO_2 flux from the Bárðarbunga volcanic system is the largest measured so far for a basaltic fissure eruption. With a maximum SO_2 flux reaching 4000 kg/s during the major degassing phase in early September 2014, degassing at Holuhraun appears to be 1 order of magnitude lower than that estimated for flood basalts [*Self et al.*, 2006] but in the range estimated for the Laki 1783–1984 eruption (50–5000 kg/s [*Thordarson and Self*, 2003]). The total SO_2 burden during the Laki eruption was estimated at 120 Tg in approximately 250 days [*Thordarson et al.*, 1996] which exceeds by 1 order of magnitude that of the eruption at Holuhraun (10.4 Tg in 180 days, see previous section). Meanwhile, the Laki eruption produced about 15 km^3 of magma [*Thordarson and Self*, 2003], also 10 times more than the eruption at Holuhraun [*Gíslason et al.*, 2015]. This suggests a similar yield for sulfur degassing at these two magmatic systems producing tholeiitic basalts.

5.2. Metal Degassing and Intrinsic Volatility of Trace Elements

The relative enrichment factor (EF) critically depends on the choice of the normalizing element (see Text S1). The use of either emanation coefficients ε or liquid-gas partition coefficients D is thus preferred. The ε values vary between 0 for refractory elements with no affinity for the vapor phase to 100% for elements that are completely lost from the magma upon degassing [*Pennisi et al.*, 1988; *Rubin*, 1997]. The ε values for any trace element are usually determined from ε_{Pb} (frequently around 1%). The ε_{Pb} can be computed from ($^{210}Po/^{210}Pb$) in a gas phase released from a magma batch in ^{210}Po-^{210}Pb radioactive equilibrium prior to degassing [*Lambert et al.*, 1985; *Gauthier et al.*, 2000]. However, at Holuhraun, the low $(^{210}Po/^{210}Pb)_0$ of 6.4 suggests that polonium might have been lost prior to eruption and thus cannot be used to determine ε_{Pb}.

The liquid-gas partition coefficient D for a trace element X is given by the concentration in gas over that in lava $[X]_G/[X]_L$. However, concentrations in the pure (undiluted) gas phase are unknown since they can only be measured in the diluted plume. The determination of D thus requires estimating the dilution factor d of the magmatic gas in the eruptive plume. This can be achieved by measuring SO_2 concentrations in the diluted plume (this study) and in the gas phase using Fourier transform infrared measurements or MultiGas sensor analyses. Liquid-gas partition coefficients can then be calculated from concentrations in the diluted plume (subscript P) using

$$D_X = \frac{[X]_P \times \frac{[SO_2]_G}{[SO_2]_P}}{[X]_L} \quad (7)$$

The SO_2 concentration in the Holuhraun gas phase was estimated close to 30% [*Gíslason et al.*, 2015], in good agreement with other hot spot-related volcanoes [*Symonds et al.*, 1994]. Based on both SO_2 and trace element concentrations in the diluted plume sample BAR-B and the average lava composition (Table 1), liquid-gas partition coefficients are determined for the Holuhraun case and are given in Table 1. Based on the D value, trace elements can be ranked as highly volatile ($D > 1$; Te, Se, and Re), moderately volatile ($0.1 < D < 1$; Bi, Cd, and Tl), or weakly to poorly volatile ($D < 0.1$; Pb, As, In, Sn, Sb, Ag, Mo, Zn, W, and Cu). This classification matches a recent compilation of D values [*Mather*, 2015, and references therein] although partition coefficients appear systematically lower in the present case. For instance, the liquid-gas partition coefficient of Pb, $D_{Pb} = 0.077$, is significantly lower than its first determination made for the plume of Stromboli ($D_{Pb} = 0.33$ [*Gauthier et al.*, 2000]), suggesting less volatility of lead as well as other trace elements in Holuhraun magma.

Both partition coefficients D and emanation coefficients ε are linked by the following relation (obtained by inverting equation A1 in *Gauthier et al.* [2000]):

$$D_X = \frac{(1-\alpha)\times\varepsilon_X}{\alpha\times(1-\varepsilon_X)} \quad (8)$$

where α is the amount of major volatiles initially dissolved in the magma and ultimately released in the gas phase. This parameter can be estimated from volatile concentrations in MI versus outgassed lava. For the present case, the α is estimated close to 0.7% [*Bali et al.*, 2015; this work]. Using equation (8), ε_{Pb} averages 0.054%, significantly lower than the commonly found 1%, but in phase with limited chlorine degassing at Holuhraun. Emanation coefficients for all siderophile and chalcophile trace elements can be determined in the same way by using either successively equations (7) and (8) or a simple mass balance equation with the ε_{Pb} value [*Pennisi et al.*, 1988]. These coefficients at Holuhraun are given in Table 1 and can be compared with known estimates from two volcanoes related to the Tyrrhenian subduction zone (Figure 7), namely, Stromboli [*Allard et al.*, 2000] and Etna (emanation coefficients calculated from data in *Aiuppa et al.* [2003], with ε_{Sn} taken from *Gauthier and Le Cloarec* [1998]). Except for Te, which concentration in both Stromboli and Etna lavas might be overestimated, hence leading to anomalously low ε values, it can be readily seen in Figure 7 that all trace elements are significantly less volatile at Holuhraun, by 1–2 orders of magnitude or more. The least volatile metals, such as W, Cu, Zn, and Mo are over 1000 times more volatile at Etna and Stromboli. This observation strongly contrasts with the very similar degassing pattern observed among hot spot volcanoes (Figure 5). It thus appears that metal volatility strongly depends on the geodynamical setting of the volcano. Gases from convergent margin volcanoes are significantly enriched in chlorine [*Symonds et al.*, 1994], in part presumably due to seawater subduction. They are thus characterized by low S/Cl ratios, as observed at Stromboli and Etna [*Allard et al.*, 2000; *Aiuppa et al.*, 2002]. In contrast, the parental magma at Holuhraun is rather chlorine poor, and limited chlorine degassing produces gases with high S/Cl ratios like at other hot spot volcanoes [e.g., *Mather et al.*, 2012; *Zelenski et al.*, 2013]. High S/Cl ratios and low Cl content of volcanic gases readily explain the lower volatility of trace metals at Holuhraun and other hot spot-related volcanoes. It further underscores the major role played by chlorides in the transport and degassing of trace elements at active volcanoes as previously observed [e.g., *Gemmell*, 1987; *Moune et al.*, 2010].

5.3. Trace Element Fluxes From Gaseous Emissions at Holuhraun

Trace element fluxes released during degassing activity at Holuhraun may be determined from the $[X]/[SO_2]$ concentration ratio in the diluted plume scaled to the SO_2 output. Because the composition of the gas phase

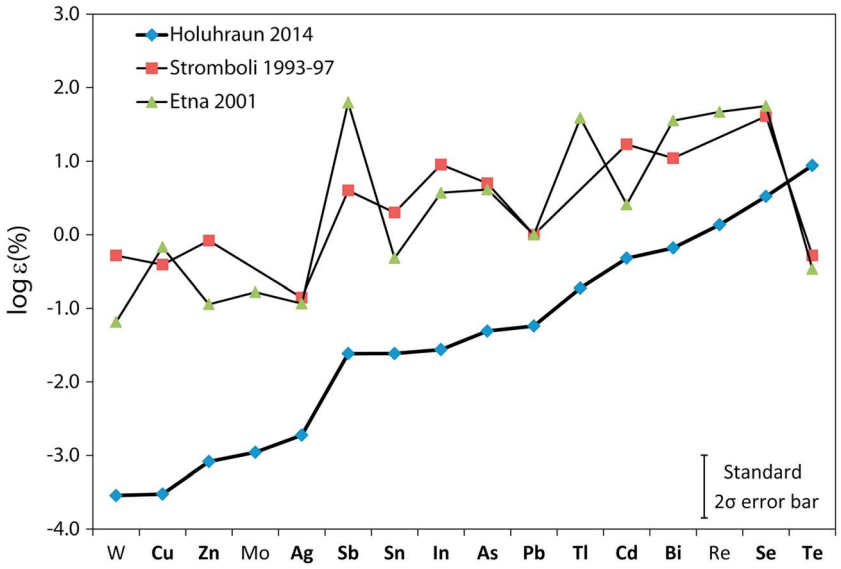

Figure 7. Emanation coefficients (ε) of trace metals for Holuhraun, Etna, and Stromboli showing contrasting and lower volatility of chalcophile (bold) and siderophile (light) metals, explained by low chlorine degassing at Holuhraun relative to subduction zone volcanoes (see text for further explanation).

most likely remained constant during the eruption [*Gíslason et al.*, 2015], it is justified to combine the concentration ratios obtained for the sample BAR-B (sample BAR-A is not used for calculations since it reached saturation for SO_2; see section 4.2.1) with the 3-month averaged SO_2 fluxes. The average SO_2 flux from the satellite data and the petrologic method is 1130 kg/s (~97,500 t/d), and the elemental fluxes are given in Table 1. These fluxes are obviously constrained by both the abundance of a given element in the magma and its intrinsic volatility. They are as low as 12 g/d for W but reach values close to 50 kg/d for Cd. The degassing at Holuhraun, therefore, was a major source of pollution to the local environment and atmosphere over Iceland. For instance, approximately 6 t of highly poisonous Cd were released to the atmosphere in 2014. The dispersion of the gas plume over inhabited areas in Iceland and its health impact on populations is beyond the scope of this paper, but the result of this study suggests that local populations were exposed not only to a large burden of noxious acidic gases but also to significant amounts of very toxic trace metals.

Trace element fluxes released by the Holuhraun eruption are compared in Figure 8 with those emitted by Erta Ale [*Zelenski et al.*, 2013], Kīlauea [*Mather et al.*, 2012] and Etna (fluxes calculated from data in *Aiuppa et al.* [2002, 2003] and *Salerno et al.* [2005]). Despite a few irregularities which may be explained by subtle differences in both metal volatility (Figure 5) and trace element abundance in lavas, the first order observation is that the fluxes at Holuhraun are approximately 7 and 70 times higher than those at Kīlauea and Erta Ale, respectively. These results emphasize the role of large basaltic fissure eruptions in the atmospheric and environmental mass loading of sulfur and volatile metals. The Holuhraun-to-Etna flux ratio for the metals and metalloids is much more scattered, reflecting both significant differences in magma composition at the two volcanoes and contrasted degassing patterns in different geodynamic settings. Although SO_2 fluxes are 1 order of magnitude higher at Holuhraun than at Etna, trace metal fluxes from Etna are on average 6 times larger than those observed at Holuhraun. This observation supports the importance of chlorine degassing in mobilizing trace metals in volcanic gases, especially the siderophile and chalcophile elements.

5.4. Possible Magma Dynamics Beneath the Holuhraun Eruptive Fissure

Short-lived radioactive disequilibria between ^{210}Pb, ^{210}Bi, and ^{210}Po measured in the gas phase may constrain magma dynamics at shallow depth. The $(^{210}Bi/^{210}Pb)_0$ activity ratio of 11.5 (Figure 6b) measured in the gas is indistinguishable from the emanation coefficient ratio ($\varepsilon_{Bi}/\varepsilon_{Pb} = 11.7$). According to the theoretical

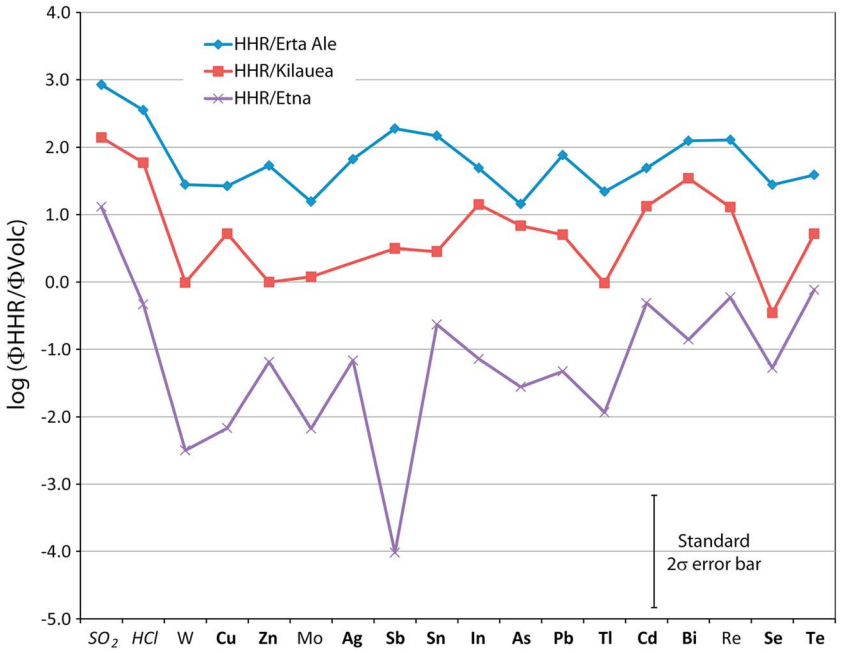

Figure 8. Sulfur, chlorine, chalcophile (bold), and siderophile (light) trace element fluxes at Holuhraun (Φ_{HHR}) normalized to those at other volcanoes (Φ_{VOLC}) including Erta Ale, Kīlauea, and Etna, illustrating the relatively large flux at Holuhraun.

degassing model proposed by *Gauthier et al.* [2000], it implies that the residence time of the degassing magma within the feeding conduit or dyke is short enough (a few days at most) to prevent significant ^{210}Bi radiogenic ingrowth. It also implies that gases are almost instantaneously transferred from the magma to the surface (less than an hour) preventing ^{210}Bi decaying within gas bubbles. In other words, the degassing process responsible for the ^{210}Bi-^{210}Pb disequilibrium most likely occurs at shallow depth where H_2O and SO_2 exsolve from ascending magma shortly before feeding the eruptive fissure. When, and only when, this condition is met, the $(^{210}Po/^{210}Pb)_0$ of a primary magmatic gas from a parental magma in radioactive equilibrium is also equal to the $\varepsilon_{Po}/\varepsilon_{Pb}$ ratio. The measured $(^{210}Po/^{210}Pb)_0$ ratio of 6.4 would thus require an ε_{Po} of 0.35%, which is quite unrealistic given the complete Po degassing observed in basaltic eruptions [e.g., *Sigmarsson et al.*, 2015]. Such a low disequilibrium ratio thus suggests that magma feeding the eruption had previously lost its polonium. Apart from its extreme affinity for the gas phase [e.g., *Gill et al.*, 1985], almost nothing is known about the geochemical behavior of polonium in magmatic systems. Nevertheless, two hypotheses can be proposed to explain the initial polonium depletion of the magma. Because polonium is expected to behave as a chalcophile element, the occurrence of sulfide globules in the Holuhraun magmatic system might act as a sink for Po. Measurements of polonium in sulfide separates are needed in order to check the validity of this hypothesis. Alternatively, the anomalously low ^{210}Po excess over ^{210}Pb could be taken to suggest an earlier degassing event. Among major volatile species, CO_2 is likely to degas first and volatile concentration measurements in melt inclusions [*Bali et al.*, 2015] suggest a depth of CO_2 exsolution greater than 9 km. Assuming that Po was first extracted at depth from the magma in a CO_2-rich gas phase, this deep degassing event must have taken place elsewhere than beneath the eruption site; otherwise, polonium would be found in gases sampled from the eruptive fissure. This is further confirmed by low CO_2/SO_2 in volcanic gases at the eruption site [*Gíslason et al.*, 2015], which suggests that CO_2 was lost during an early degassing stage. These observations could be tentatively reconciled by assuming that the initial degassing event occurred at depth somewhere along the rifting path from the Bárðarbunga central volcano to the eruption site.

Regardless of the exact mechanism causing the initial polonium depletion at depth, a quantitative polonium loss like in other basaltic systems may be assumed, resulting in $(^{210}Po) = 0$ in the magma before feeding the eruption fissure. The low (^{210}Po) activity measured in the gas phase could then be explained by radiogenic ingrowth of ^{210}Po atoms in the magma between the Po depletion locality (somewhere at depth beneath

the Bárðarbunga volcanic system) and the site of final degassing event (close to the surface under Holuhraun). The (^{210}Pb) activity in the lava is estimated at 3.8 Bq/kg (O. Sigmarsson, Calculated from α-spectrometric analyses of ^{210}Pb progeny, ^{210}Po, unpublished data, 2015). For $\varepsilon_{Po} = 100\%$, the $(^{210}Po/^{210}Pb)_0$ activity ratio of 6.4 in the gas phase thus requires $(^{210}Po)_L = 0.013$ Bq/kg in the magma prior to final degassing at Holuhraun. Using a classic radioactivity law between grandparent, parent, and daughter products (namely, ^{210}Pb, ^{210}Bi, and ^{210}Po, respectively) such as given in *Bourdon et al.* [2003], we calculate that such an activity was reached 16.6 h after the initial fractionation. It thus appears that the magma was rapidly transferred to the surface. Based on the deepest earthquakes recorded during dyke propagation [*Sigmundsson et al.*, 2015], the pressure of partial CO_2 degassing [*Bali et al.*, 2015], and the thermobarometry of clinopyroxene crystallization [*Haddadi et al.*, 2015], the fractionation can be assumed to have occurred at a depth of at least 10 km beneath the Bárðarbunga central volcano. The magma had thus to migrate over about 45 km before feeding the eruptive fissure. It represents an average magma transfer rate of 0.75 m/s, in good agreement with previous determinations on Hawai'ian eruptions [*Parfitt*, 2004, and references therein]. Recent work on passive degassing at Kīlauea volcano also suggests magma transfer rate in the range 0.02–0.4 m/s [*Edmonds et al.*, 2013]. Although their maximum estimate closely matches the value obtained here, the higher magma transfer rate at Bárðarbunga is thought to reflect the more sustained magma dynamics during this large effusive event. This magma propagation rate further compares with the dyke propagation rate prior to the eruption. Instantaneous propagation rates may have been as high as 0.28 m/s [*Sigmundsson et al.*, 2015]. However, considering that it took almost 2 weeks to rift the whole distance from Bárðarbunga to the eruption site, the averaged magma transfer rate (0.04 m/s), if equal to the seismic propagation rate, appears to be 1 order of magnitude lower before the beginning of the eruption than after. This is readily explained by the fact that magma travels faster once the dyke system is fully opened.

6. Conclusion

The 2014–2015 eruption at Holuhraun produced approximately 1.6 km^3 of olivine tholeiitic magma and prodigious amounts of gas released into the atmosphere. We have quantified the SO_2 fluxes during the first 3 months of the eruption using two complementary and independent approaches, namely, a high-resolution time series of MSG-SEVIRI satellite data and the petrologic method based on both initial S contents measured in melt inclusions and residual S contents preserved in the most degassed products. Both methods reveal similar SO_2 fluxes (1200 kg/s and 1050 kg/s), which suggest that all the degassing magma at depth contributed to the eruption and the gas budget, a pattern observed at other hot spot volcanoes. Further agreement between the SO_2 fluxes measured in this study and other OMI-derived and DOAS estimates suggests that MSG-SEVIRI and the associated monitoring system (HOTVOLC) are important tools for remote sensing in volcanology. The high temporal resolution of this IR sensor is perfectly suitable to monitor long-lasting basaltic eruptions and is able to provide, in real time with only little gaps, quantitative parameters on both the degassing process and the plume dynamics. Furthermore, by picturing the gas plume close to the source vent, high-resolution time series from MSG-SEVIRI make easier the calculation of SO_2 mass fluxes since negligible *e*-folding time can be assumed in these conditions.

The SO_2 flux at the Bárðarbunga volcanic system is the largest still measured for basaltic fissure eruptions. It exceeds by a factor 4 to 10 the current flux at Kīlauea, Hawai'i. The total SO_2 atmospheric loading during this eruption is estimated at more than 10 Tg. It represents only 10% of the SO_2 burden from the 1783–1984 Laki eruption, which also produced 10 times more lava (15 km^3). Both magmatic systems appear quite comparable in terms of SO_2 degassing efficiency, which makes the Holuhraun eruption a small Laki event.

Gas and aerosol samples were taken in the plume released from the main craters and were subsequently analyzed for major gas species, trace elements, and radioactive isotopes. High S/Cl mass ratios (40–52) were measured in the gas samples, suggesting limited Cl degassing at Holuhraun already observed at other hot spot-related volcanoes. Similar ratios of S/Cl were calculated by scaling concentrations in melt inclusions to those in the degassed lava, which suggests concurrent degassing of Cl and S at shallow depth beneath the eruption site. All analyzed chalcophile and siderophile elements appear moderately to highly volatile in the gas plume at Holuhraun with enrichment factors relative to Mg up to 10^6 for the most volatile element, Te. Similar degassing patterns are observed for Kīlauea, Erta Ale, and Bárðarbunga, suggesting a singular mode of metal degassing occurring at hot spot volcanoes. In contrast, metal degassing at subduction volcanoes (Etna, Stromboli) is significantly different and metal volatility at Holuhraun is 2–3 orders of magnitude lower.

Although further work on metal speciation in volcanic gases from hot spot volcanoes is needed, this contrasted behavior might be related to enhanced chlorine degassing at subduction zone related volcanoes.

Short-lived radioactive disequilibria between ^{210}Pb, ^{210}Bi, and ^{210}Po in the volcanic plume of Holuhraun are characterized by normal $(^{210}Bi/^{210}Pb)_0$ but an order of magnitude lower $(^{210}Po/^{210}Pb)_0$ than observed elsewhere, suggesting polonium depletion prior to eruption. This is best explained by a two-step degassing process where the most volatile ^{210}Po is lost upon early CO_2 degassing at depth beneath the Bárðarbunga central volcano, prior to final degassing of SO_2 and HCl at shallow depth beneath the Holuhraun eruption site. In such a scenario, the very low (^{210}Po) activity in the diluted plume (6.56 mBq/m^3) can be explained by radioactive ingrowth of ^{210}Po from its parent in the CO_2-depleted magma en route to the eruption site, leading to a magma transfer rate of 0.75 m/s.

Acknowledgments

We are grateful to the Field Team at IES for their help during lava and gas sampling. Mhammed Benbakkar (ICP-AES), Jean-Luc Devidal (electron microprobe), Claire Fonquernie (CHNS/O analyzer), and Jean-Luc Piro and Krzysztof Suchorski (ICP-MS), all from LMV, are acknowledged for their help with analytical techniques. Analytical and publication costs were covered by the ANR project "DeGazMag" of the French government. The TOSCA program of the Centre National d'Etudes Spatiales (CNES, France) supported this work through the convention CNES/ 92532-BC-T39. SEVIRI data were provided by the HOTVOLC reception platform (OPGC) through agreement with EUMETSAT and Météo-France. We are grateful to Örvar Atli Þorgeirsson (Arctic Photo, Reykjavík, Iceland) for having shared one of his wonderful pictures of the eruption (more can be seen at his website http://www.arctic-photo.is/volcanic). The data used in this paper are available upon request from the corresponding author at P.J. Gauthier@opgc.fr. This paper benefitted from careful reviews by Mike Poland and two anonymous reviewers. This is ClerVolc contribution 192.

References

Aiuppa, A., C. Federico, A. Paonita, G. Pecoraino, and M. Valenza (2002), S, Cl and F degassing as an indicator of volcanic dynamics: The 2001 eruption of Mount Etna, *Geophys. Res. Lett.*, *29*(11), 1556, doi:10.1029/2002GL015032.

Aiuppa, A., G. Dongarrà, M. Valenza, C. Federico, and G. Pecoraino (2003), Degassing of trace volatile metals during the 2001 eruption of Etna, in *Volcanism and the Earth's Atmosphere*, *Geophys. Monogr. Ser.*, vol. 139, edited by A. Robock and C. Oppenheimer, pp. 41–54, AGU, Washington, D. C., doi:10.1029/139GM03.

Allard, P. (1997), Endogenous magma degassing and storage at Mount Etna, *Geophys. Res. Lett.*, *24*, 2219–2222, doi:10.1029/97GL02101.

Allard, P., A. Aiuppa, H. Loyer, F. Carrot, A. Gaudry, G. Pinte, A. Michel, and G. Dongarrà (2000), Acid gas and metal emission rates during long-lived basalt degassing at Stromboli volcano, *Geophys. Res. Lett.*, *27*, 1207–1210, doi:10.1029/1999GL008413.

Allard, P., et al. (2015), Prodigious emission rates and magma degassing budget of major, trace and radioactive volatile species from Ambrym basaltic volcano, Vanuatu island arc, *J. Volcanol. Geotherm. Res.*, doi:10.1016/j.jvolgeores.2015.10.004, in press.

Allen, A. G., P. J. Baxter, and C. J. Ottley (2000), Gas and particle emissions from Soufrière Hills volcano, Montserrat, West Indies: Characterization and health hazard assessment, *Bull. Volcanol.*, *62*, 8–19, doi:10.1007/s004450050287.

Bali, E., O. Sigmarsson, S. Jakobsson, and H. Gunnarsson (2015), Volatile-budget of the new fissure eruption of the Barðarbunga system, Iceland, *Geophys. Res. Abstr.*, *17*, EGU2015-5757.

Beirle, S., C. Hörmann, M. Penning de Vries, S. Dörner, C. Kern, and T. Wagner (2014), Estimating the volcanic emission rate and atmospheric lifetime of SO_2 from space: A case study for Kīlauea volcano, Hawai'i, *Atmos. Chem. Phys.*, *14*, 8309–8322, doi:10.5194/acp-14-8309-2014.

Boichu, M., C. Oppenheimer, V. Tsanevand, and P. R. Kyle (2010), High temporal resolution SO_2 flux measurements at Erebus volcano, Antarctica, *J. Volcanol. Geotherm. Res.*, *190*, 325–336, doi:10.1016/j.jvolgeores.2009.11.020.

Bourdon, B., S. Turner, G. M. Henderson, and C. C. Lundstrom (2003), Introduction to U-series geochemistry *in*: Bourdon, B., G.M. Henderson., C.C. Lundstrom and S. Turner (Eds) Uranium-Series Geochemistry, *Rev. Mineral. Geochem.*, *52*, 1–21, doi:10.2113/0520001.

Carboni, E., R. Grainger, J. Walker, A. Dudhia, and R. Siddans (2012), A new scheme for sulphur dioxide retrieval from IASI measurements: Application to the Eyjafjallajökull eruption of April and May 2010, *Atmos. Chem. Phys.*, *12*, 11,417–11,434, doi:10.5194/acp-12-11417-2012.

Carroll, M. R., and M. J. Rutherford (1988), Sulfur speciation in hydrous experimental glasses of varying oxidation states: Results from measured wavelength shifts of sulfur X-rays, *Am. Mineral.*, *73*, 845–849.

Corradini, S., L. Merucci, and A. J. Prata (2009), Retrieval of SO_2 from thermal infrared satellite measurements: Correction procedures for the effects of volcanic ash, *Atmos. Meas. Tech.*, *2*, 177–191, doi:10.5194/amt-2-177-2009.

Devine, J. D., H. Sigurdsson, A. N. Davis, and S. Self (1984), Estimate of sulfur and chlorine yield to the atmosphere from volcanic eruptions and potential climatic effects, *J. Geophys. Res.*, *89*, 6309–6325, doi:10.1029/JB089iB07p06309.

Eckhardt, S., A. J. Prata, P. Seibert, K. Stebel, and A. Stohl (2008), Estimation of the vertical profile of sulfur dioxide injection into the atmosphere by a volcanic eruption using satellite column measurements and inverse transport modeling, *Atmos. Chem. Phys.*, *8*, 3881–3897, doi:10.5194/acp-8-3881-2008.

Edmonds, M., et al. (2013), Magma storage, transport and degassing during the 2008–10 summit eruption at Kīlauea Volcano, Hawai'i, *Geochim. Cosmochim. Acta*, *123*, 284–301, doi:10.1016/j.gca.2013.05.038.

Elias, T., and A. J. Sutton (2012), Sulfur dioxide emission rates from Kīlauea Volcano, Hawai'i, 2007–2010, *U.S. Geol. Surv. Open-File Rep.*, 2012–1107, 25 pp. [available at http://pubs.usgs.gov/of/2012/1107/.]

Frogner, P., S. R. Gíslason, and N. Oskarsson (2001), Fertilizing potential of volcanic ash in ocean surface water, *Geology*, *29*, 487–490, doi:10.1130/0091-7613(2001)029.

Gauthier, P.-J., and M.-F. Le Cloarec (1998), Variability of alkali and heavy metal fluxes released by Mt. Etna volcano, Sicily, between 1991 and 1995, *J. Volcanol. Geotherm. Res.*, *81*, 311–326, doi:10.1016/S0377-0273(98)00002-X.

Gauthier, P.-J., M.-F. Le Cloarec, and M. Condomines (2000), Degassing processes at Stromboli volcano inferred from short-lived disequilibria (^{210}Pb-^{210}Bi-^{210}Po) in volcanic gases, *J. Volcanol. Geotherm. Res.*, *102*, 1–19, doi:10.1016/S0377-0273(00)00179-7.

Gemmell, J. B. (1987), Geochemistry of metallic trace elements in fumarolic condensates from Nicaraguan and Costa Rican volcanoes, *J. Volcanol. Geotherm. Res.*, *33*, 161–181, doi:10.1016/0377-0273(87)90059-X.

Gill, J., R. Williams, and K. Bruland (1985), Eruption of basalt and andesite lava degasses ^{222}Rn and ^{210}Po, *Geophys. Res. Lett.*, *12*, 17–20, doi:10.1029/GL012i001p00017.

Gíslason, S. R., et al. (2015), Environmental pressure from the 2014–15 eruption of Bárðarbunga volcano, Iceland, *Geochem. Persp. Lett.*, *1*, 84–93, doi:10.7185/geochemlet.1509.

Gouhier, M., and D. Coppola (2011), Satellite-based evidence for a large hydrothermal system at Piton de la Fournaise volcano (Reunion Island), *Geophys. Res. Lett.*, *38*, L02302, doi:10.1029/2010GL046183.

Gouhier, M., P.-J. Gauthier, B. Haddadi, S. Moune, and O. Sigmarsson (2015), Retrieval of lava and SO_2 fluxes during long-lived effusive eruptions using MSG-SEVIRI: The case of Bardarbunga 2014 activity, *Geophys. Res. Abstr.*, *17*, EGU2015-9955.

Gouhier, M., Y. Guéhenneux, P. Labazuy, P. Cacault, J. Decriem, and S. Rivet (2016), HOTVOLC: A web-based monitoring system for volcanic hot spots, in *Detecting, Modelling and Responding to Effusive Eruptions*, edited by A. J. L. Harris et al., *Geol. Soc. London Spec. Publ.*, *426*, doi:10.1144/SP426.31, in press.

Grahn, H., P. von Schoenberg, and N. Brännström (2015), What's that smell? Hydrogen sulphide transport from Bárðarbunga to Scandinavia, *J. Volcanol. Geotherm. Res.*, *303*, 187–192, doi:10.1016/j.jvolgeores.2015.07.006.

Gudmundsson, A., N. Lecoeur, N. Mohajeri, and T. Thordarson (2014), Dike emplacement at Bárðarbunga, Iceland, induces unusual stress changes, caldera deformation, and earthquakes, *Bull. Volcanol.*, *76*, 869–875, doi:10.1007/s00445-014-0869-8.

Haddadi, B., O. Sigmarsson, and J.-L. Devidal (2015), Determining intensive parameters through clinopyroxene-liquid equilibrium in Grimsvötn 2011 and Bárðarbunga 2014 basalts, *Geophys. Res. Abstr.*, *17*, EGU2015-5791.

Hjartarson, Á. (1988), Þjórsárhraunið mikla—stærsta nútímahraun jarðar. (The Great Thjorsa lava—largest Holocene lava field on Earth), *Náttúrufræðingurinn*, *58*, 1–16.

Jugo, P. J., M. Wilke, and R. E. Botcharnikov (2010), Sulfur K-edge XANES analysis of natural and synthetic basaltic glasses: Implications for S speciation and S content as function of oxygen fugacity, *Geochim. Cosmochim. Acta*, *74*, 5926–5938, doi:10.1016/j.gca.2010.07.022.

Karagulian, F., L. Clarisse, C. Clerbaux, A. J. Prata, D. Hurtmans, and P.-F. Coheur (2010), Detection of volcanic SO_2, ash, and H_2SO_4 using the Infrared Atmospheric Sounding Interferometer (IASI), *J. Geophys. Res.*, *115*, D00L02, doi:10.1029/2009JD012786.

König, S., A. Luguet, J.-P. Lorand, F. Wombacher, and M. Lissner (2012), Selenium and tellurium systematics of the Earth's mantle from high precision analyses of ultra-depleted orogenic peridotites, *Geochim. Cosmochim. Acta*, *86*, 354–366, doi:10.1016/j.gca.2012.03.014.

Krotkov, N. A., M. R. Schoeberl, G. A. Morris, S. Carn, and K. Yang (2010), Dispersion and lifetime of the SO_2 cloud from the August 2008 Kasatochi eruption, *J. Geophys. Res.*, *115*, D00L20, doi:10.1029/2010JD013984.

Krueger, A. J., C. C. Schnetzler, and L. S. Walter (1996), The December 1981 eruption of Nyamuragira volcano (Zaire), and the origin of the 'mystery cloud' of early 1982, *J. Geophys. Res.*, *101*, 15,191–15,196, doi:10.1029/96JD00221.

Labazuy, P., M. Gouhier, A. Harris, Y. Guéhenneux, M. Hervo, J.-C. Bergès, P. Cacault, and S. Rivet (2012), Near real-time monitoring of the April–May 2010 Eyjafjallajökull ash cloud: An example of a web-based, satellite data-driven reporting system, *Int. J. Environ. Pollut.*, *48–1/4*, 262–272, doi:10.1504/IJEP.2012.049673.

Lambert, G., P. Bristeau, and G. Polian (1976), Emission and enrichments of radon daughters from Etna volcano magma, *Geophys. Res. Lett.*, *3–12*, 724–726, doi:10.1029/GL003i012p00724.

Lambert, G., M.-F. Le Cloarec, B. Ardouin, and J. C. Le Roulley (1985), Volcanic emission of radionuclides and magma dynamics, *Earth Planet. Sci. Lett.*, *76*, 185–192, doi:10.1016/0012-821X(85)90158-X.

Le Cloarec, M.-F., and P.-J. Gauthier (2003), Merapi volcano, Central Java, Indonesia: A case study of radionuclide behavior in volcanic gases and its implications for magma dynamics at andesitic volcanoes, *J. Geophys. Res.*, *108*(B5), 2243, doi:10.1029/2001JB001709.

Lopez, T. M., S. A. Carn, C. Werner, P. Kelly, M. Doukas, M. Pfeffer, D. Fee, P. Webley, C. Cahill, and D. J. Schneider (2013), Evaluation of Redoubt volcano's sulfur dioxide emissions by the Ozone Monitoring Instrument, *J. Volcanol. Geotherm. Res.*, *259*, 290–307, doi:10.1016/j.jvolgeores.2012.03.002.

Luhr, J. F., I. S. E. Carmichael, and J. C. Varekamp (1984), The 1982 eruptions of El Chichòn volcano, Chiapas, Mexico: Mineralogy and petrology of the anhydrite bearing pumices, *J. Volcanol. Geotherm. Res.*, *23*, 69–108, doi:10.1016/0377-0273(84)90057-X.

Mather, T. A. (2015), Volcanoes and the environment: Lessons for understanding Earth's past and future from studies of present-day volcanic emissions, *J. Volcanol. Geotherm. Res.*, *304*, 160–179, doi:10.1016/j.jvolgeores.2015.08.016.

Mather, T. A., D. M. Pyle, and T. H. E. Heaton (2008), Investigation of the use of filter packs to measure the sulphur isotopic composition of volcanic sulphur dioxide and the sulphur and oxygen isotopic composition of volcanic sulphate aerosol, *Atmos. Env.*, *42*, 4611–4618, doi:10.1016/j.atmosenv.2008.01.052.

Mather, T. A., et al. (2012), Halogens and trace metal emissions from the on-going 2008 summit eruption of Kīlauea volcano, Hawai'i, *Geochim. Cosmochim. Acta*, *83*, 292–323, doi:10.1016/j.gca.2011.11.029.

McGonigle, A. J. S., P. Delmelle, C. Oppenheimer, V. I. Tsanev, T. Delfosse, G. Williams-Jones, K. Horton, and T. A. Mather (2004), SO_2 depletion in tropospheric volcanic plumes, *Geophys. Res. Lett.*, *31*, L13201, doi:10.1029/2004GL019990.

Ménard, G., S. Moune, I. Vlastélic, F. Aguilera, S. Valade, M. Bontemps, and R. González (2014), Gas and aerosol emissions from Lascar volacno (Northern Chile): Insights into the origin of gases and their links with the volcanic activity, *J. Volcanol. Geotherm. Res.*, *287*, 51–67, doi:10.1016/j.jvolgeores.2014.09.004.

Merucci, L., M. R. Burton, S. Corradini, and G. G. Salerno (2011), Reconstruction of SO_2 flux emission chronology from space-based measurements, *J. Volcanol. Geotherm. Res.*, *206*, 80–87, doi:10.1016/j.jvolgeores.2011.07.002.

Moune, S., P.-J. Gauthier, S. R. Gíslason, and O. Sigmarsson (2006), Trace element degassing and enrichment in the eruptive plume of Hekla volcano (Iceland) during the 2000 eruption, *Geochim. Cosmochim. Acta*, *70*, 461–479, doi:10.1016/j.gca.2005.09.011.

Moune, S., O. Sigmarsson, T. Thordarson, and P.-J. Gauthier (2007), Recent volatile evolution in the magmatic system of Hekla volcano, Iceland, *Earth Planet. Sci. Lett.*, *255*, 373–389, doi:10.1016/j.epsl.2006.12.024.

Moune, S., P.-J. Gauthier, and P. Delmelle (2010), Trace elements in the particulate phase of the plume of Masaya Volcano, Nicaragua, *J. Volcanol. Geotherm. Res.*, *193*(3–4), 232–244, doi:10.1016/j.jvolgeores.2010.04.004.

Moune, S., O. Sigmarsson, P. Schiano, T. Thordarson, and J. Keiding (2012), Melt inclusion constraints on the magma source of Eyjafjallajökull 2010 flank eruption, *J. Geophys. Res.*, *117*, B00C07, doi:10.1029/2011JB008718.

Óladóttir, B., O. Sigmarsson, G. Larsen, and J.-L. Devidal (2011), Provenance of basaltic tephra from Vatnajökull subglacial volcanoes, Iceland, as determined by major- and trace-element analyses, *Holocene*, *21*, 1037–1048, doi:10.1177/0959683611400456.

Óladóttir, B., G. Larsen, and O. Sigmarsson (2012), Deciphering eruption history and magmatic processes from tephra in Iceland, *Jökull*, *62*, 21–38.

Oppenheimer, C., A. J. S. McGonigle, P. Allard, M. J. Wooster, and V. Tsanev (2004), Sulfur, heat, and magma budget of Erta 'Ale lava lake, Ethiopia, *Geology*, *32*, 509–512, doi:10.1130/G20281.1.

Parfitt, E. A. (2004), A discussion of the mechanisms of explosive basaltic eruptions, *J. Volcanol. Geotherm. Res.*, *134*, 77–107, doi:10.1016/j.jvolgeores.2004.01.002.

Pennisi, M., M.-F. Le Cloarec, G. Lambert, and J.-C. Le Roulley (1988), Fractionation of metals in volcanic emissions, *Earth Planet. Sci. Lett.*, *88*, 284–288, doi:10.1016/0012-821X(88)90085-4.

Prata, A., and J. Kerkmann (2007), Simultaneous retrieval of volcanic ash and SO_2 using MSG-SEVIRI measurements, *Geophys. Res. Lett.*, *34*, L05813, doi:10.1029/2006GL028691.

Prata, A. J., W. I. Rose, S. Self, and D. M. O'Brien (2003), Global, long-term sulphur dioxide measurements from TOVS data: A new tool for studying explosive volcanism and climate, in *Volcanism and the Earth's Atmosphere*, *Geophys. Monogr. Ser.*, vol. 139, edited by A. Robock and C. Oppenheimer, pp. 75–92, AGU, Washington, D. C., doi:10.1029/139GM05.

Pyle, D. M., T. A. Mather, and J. Biggs (2013), Remote sensing of volcanoes and volcanic processes: Integrating observation and modelling—Introduction*in* Pyle, D.M., T.A. Mather, and J. Biggs (Eds) Remote Sensing of Volcanoes and Volcanic Processes: Integrating Observation and Modelling, *Geol. Soc. London Spec. Publ.*, *380*, 1–13, doi:10.1144/SP380.14.

Realmuto, V., M. Abrams, M. Buongiorno, and D. Pieri (1994), The use of multispectral thermal infrared image data to estimate the sulfur dioxide flux from volcanoes: A case study from Mount Etna, Sicily, 29 July 1986, *J. Geophys. Res.*, *99*, 481–488, doi:10.1029/93JB02062.

Riel, B., P. Milillo, M. Simons, P. Lundgren, H. Kanamori, and S. Samsonov (2015), The collapse of Bárðarbunga caldera, Iceland, *Geophys. J. Int.*, *202*, 446–453, doi:10.1093/gji/ggv157.

Rose, W. I., et al. (2003), The February–March 2000 eruption of Hekla, Iceland from a satellite perspective, in *Volcanism and the Earth's Atmosphere*, *Geophys. Monogr. Ser.*, vol. 139, edited by A. Robock and C. Oppenheimer, pp. 107–132, AGU, Washington, D. C., doi:10.1029/139GM07.

Rose, W. I., et al. (2006), Atmospheric chemistry of a 33–34 hour old volcanic cloud from Hekla Volcano (Iceland): Insights from direct sampling and the application of chemical box modeling, *J. Geophys. Res.*, *111*, D20206, doi:10.1029/2005JD006872.

Rubin, K. H. (1997), Degassing of metals and metalloids from erupting seamount and mid-ocean ridge volcanoes: Observations and predictions, *Geochim. Cosmochim. Acta*, *61*, 3525–3542, doi:10.1016/S0016-7037(97)00179-8.

Salerno, G., T. Caltabiano, M. Burton, N. Bruno, and E. Longo (2005), Anomalous degassing rates from Mt. Etna, 2001–2005, *Geophys. Res. Abstr.*, *7*, EGU2005-10606-10607, doi:10.1029/143GM08.

Scaillet, B., J. F. Luhr, and M. R. Carroll (2003), Petrological and volcanological constraints on volcanic sulfur emissions to the atmosphere, in *Volcanism and the Earth's Atmosphere*, *Geophys. Monogr. Ser.*, vol. 139, edited by A. Robock and C. Oppenheimer, pp. 11–40, AGU, Washington, D. C., doi:10.1029/139GM02.

Schmidt, A., et al. (2015), Satellite detection, long-range transport, and air quality impacts of volcanic sulfur dioxide from the 2014–2015 flood lava eruption at Bárðarbunga (Iceland), *J. Geophys. Res. Atmos.*, *120*, 9739–9757, doi:10.1002/2015JD023638.

Self, S., M. Widdowsona, T. Thordarson, and A. E. Jay (2006), Volatile fluxes during flood basalt eruptions and potential effects on the global environment: A Deccan perspective, *Earth Planet. Sci. Lett.*, *248*, 518–532, doi:10.1016/j.epsl.2006.05.041.

Sharma, K., S. Blake, S. Self, and A. J. Krueger (2004), SO_2 emissions from basaltic eruptions, and the excess sulfur issue, *Geophys. Res. Lett.*, *31*, L13612, doi:10.1029/2004GL019688.

Sigmarsson, O., I. Vlastelic, R. Andreasen, I. Bindeman, J.-L. Devidal, S. Moune, J. K. Keiding, G. Larsen, A. Höskuldsson, and T. Thordarson (2011), Remobilization of silicic intrusion by mafic magmas during the 2010 Eyjafjallajökull eruption, *Solid Earth*, *2*, 271–281, doi:10.5194/se-2-271-2011.

Sigmarsson, O., B. Haddadi, S. Carn, S. Moune, J. Gudnason, K. Yang, and L. Clarisse (2013), The sulfur budget of the 2011 Grímsvötn eruption, Iceland, *Geophys. Res. Lett.*, *40*, 6095–6100, doi:10.1002/2013GL057760.

Sigmarsson, O., M. Condomines, and P.-J. Gauthier (2015), Excess ^{210}Po in 2010 Eyjafjallajökull tephra (Iceland): Evidence for pre-eruptive gas accumulation, *Earth Planet. Sci. Lett.*, *427*, 66–73, doi:10.1016/j.epsl.2015.06.054.

Sigmundsson, F., et al. (2015), Segmented lateral dyke growth in a rifting event at Bárðarbunga volcanic system, Iceland, *Nature*, *517*, 191–195, doi:10.1038/nature14111.

Symonds, R. B., W. I. Rose, G. J. S. Bluth, and T. M. Gerlach (1994), Volcanic-gas studies: Methods, results, and applications*in*: Carroll M.R. and J. R. Holloway (Eds) Volatiles in magmas, *Rev. Mineral. Geochem.*, *30*, 1–66.

Theys, N., et al. (2013), Volcanic SO_2 fluxes derived from satellite data: A survey using OMI, GOME-2, IASI and MODIS, *Atmos. Chem. Phys.*, *13*, 5945–5968, doi:10.5194/acp-13-5945-2013.

Thomas, H. E., I. M. Watson, C. Kearney, S. A. Carn, and S. J. Murray (2009), A multi-sensor comparison of sulphur dioxide emissions from the 2005 eruption of Sierra Negra volcano, Galápagos Islands, *Remote Sens. Environ.*, *113*, 1331–1342, doi:10.1016/j.rse.2009.02.019.

Thorarinsson, S. (1974), Vötnin stríð. Saga Skeiðarárhlaupa og Grímsvatnagosa (The swift flowing rivers. Annals of jökulhlaups in the river Skeidará and eruptions of Grímsvötn), Bókaútgáfa Menningarsjóðs, 254 pp., Reykjavik, Iceland.

Thordarson, T., and S. Self (2003), Atmospheric and environmental effects of the 1783–84 Laki eruption: A review and re-assessment, *J. Geophys. Res.*, *108*(D1), 4011, doi:10.1029/2001JD002042.

Thordarson, T., S. Self, N. Oskarsson, and T. Hulsebosch (1996), Sulfur, chlorine, and fluorine degassing and atmospheric loading by the 1783–1784 AD Laki (Skaftár Fires) eruption in Iceland, *Bull. Volcanol.*, *58*, 205–225, doi:10.1007/s004450050136.

Urai, M. (2004), Sulfur dioxide flux estimation from volcanoes using Advanced Spaceborne Thermal Emission and Reflection Radiometer: A case study of Miyakejima volcano, Japan, *J. Volcanol. Geotherm. Res.*, *134*, 1–13, doi:10.1016/j.jvolgeores.2003.11.008.

Wallace, P. J. (2005), Volatiles in subduction zone magmas: Concentrations and fluxes based on melt inclusion and volcanic gas data, *J. Volcanol. Geotherm. Res.*, *140*(1), 217–240, doi:10.1016/j.jvolgeores.2004.07.023.

Wallace, P. J., and M. Edmonds (2011), The sulfur budget in magmas: Evidence from melt inclusions, submarine glasses, and volcanic gas emissions *in*: Behrens H. and J. D. Webster (Eds) Sulfur in Magmas and Melts: Its Importance for Natural and Technical Processes, *Rev. Mineral. Geochem.*, *73*(1), 215–246, doi:10.2138/rmg.2011.73.8.

Watson, I., V. Realmuto, W. Rose, A. Prata, G. Bluth, Y. Gu, C. Bader, and T. Yu (2004), Thermal infrared remote sensing of volcanic emissions using the moderate resolution imaging spectroradiometer, *J. Volcanol. Geotherm. Res.*, *135*, 75–89, doi:10.1016/j.jvolgeores.2003.12.017.

Whitby, K. T. (1978), The physical characteristics of sulfur aerosols, *Atmos. Environ.*, *12*, 135–159, doi:10.1016/0004-6981(78)90196-8.

Zelenski, M. E., T. P. Fischer, J. M. de Moor, B. Marty, L. Zimmermann, D. Ayalew, A. N. Nekrasov, and V. K. Karandashev (2013), Trace elements in the gas emissions from the Erta-Ale volcano, Afar, Ethiopia, *Chem. Geol.*, *357*, 95–116, doi:10.1016/j.chemgeo.2013.08.022.

Zoller, W. H., E. S. Gladney, and R. A. Duce (1974), Atmospheric concentrations and sources of trace metals at the South Pole, *Science*, *183*, 198–200, doi:10.1126/science.183.4121.198.